UNITED TECHNOLOGIES RESEARCH CENTER

East Hartford, Connecticut 06108

R83-916154-1

A Study of Adherent Oxide Formation

REPORTED BY _____

A. W. Funkenbusch

J. G. Smeggil

APPROVED BY _____

N. S. Bornstein
Chief, Materials Process Research

DATE October 1983

COPY NO. _____

SECURITY CLASSIFICATION OF THIS PAGE *(When Data Entered)*

REPORT DOCUMENTATION PAGE		READ INSTRUCTIONS BEFORE COMPLETING FORM
1. REPORT NUMBER R83-916154-1	**2. GOVT ACCESSION NO.** AD-A139505	**3. RECIPIENT'S CATALOG NUMBER**
4. TITLE (and Subtitle) A Study of Adherent Oxide Formation		**5. TYPE OF REPORT & PERIOD COVERED** Annual Technical Report July 1982 – September 1983
		6. PERFORMING ORG. REPORT NUMBER
7. AUTHOR(s) A. W. Funkenbusch and J. G. Smeggil		**8. CONTRACT OR GRANT NUMBER(s)** N00014-82-C-0618
9. PERFORMING ORGANIZATION NAME AND ADDRESS United Technologies Research Center East Hartford, Connecticut 06108		**10. PROGRAM ELEMENT, PROJECT, TASK AREA & WORK UNIT NUMBERS**
11. CONTROLLING OFFICE NAME AND ADDRESS Office of Naval Research Department of the Navy Arlington, VA 22217		**12. REPORT DATE** October 1983
		13. NUMBER OF PAGES 80
14. MONITORING AGENCY NAME & ADDRESS(if different from Controlling Office)		**15. SECURITY CLASS. (of this report)** UNCLASSIFIED
		15a. DECLASSIFICATION/DOWNGRADING SCHEDULE

16. DISTRIBUTION STATEMENT (of this Report)

Reproduction in whole or in part is permitted for any purpose of the United States Government

17. DISTRIBUTION STATEMENT (of the abstract entered in Block 20, if different from Report)

18. SUPPLEMENTARY NOTES

19. KEY WORDS (Continue on reverse side if necessary and identify by block number)

Oxidation	Laser-Processing
Coatings	Minor Element Effects
Oxide Scale Adherence	Auger Electron Spectroscopy
Oxide Scale Formation	

20. ABSTRACT (Continue on reverse side if necessary and identify by block number)

The effects by which minor element additives (yttrium and hafnium) and laser surface melting and rapid solidification (laser-processing) improve oxide scale adherence to NiCrAl were investigated. Laser-processed materials were isothermally and cyclically oxidized and oxide scale structure and adherence were examined. Laser-processing promoted thin, dense oxide formation in yttrium doped samples. Results are discussed in terms of effects for improved oxide scale adherence.

DD FORM 1473 1 JAN 73   EDITION OF 1 NOV 65 IS OBSOLETE
 S/N 0102-LF-014-6601

R83-916154-1

A Study of Adherent Oxide Formation

SUMMARY

Oxide adherence is an important factor influencing the life of materials exposed at elevated temperatures. It is well established that trace quantities of reactive elements (yttrium, hafnium, etc.) greatly improve oxide adherence. Recently it has been demonstrated that further improvements in oxide adherence are possible through laser melting and rapid solidification of thin surface lasers (laser-processing). The objective of this study is to determine the effect(s) by which laser processing and minor elements improve oxide scale adhesion to nickel base turbine coating compositions.

The highlights of the first year are:

- The beneficial effects of laser-processing required the presence of minor element additions (yttrium).

- Laser processing of yttrium and hafnium modified NiCrAl altered the morphology of the alumina scale and promoted the formation of a thinner, dense protective layer.

- Thin aluminum oxide films formed on surfaces during laser processing were not responsible for subsequent improved oxide adherence.

- The mechanisms associated with pegs and pore formation were not responsible for the improvements induced by laser processing or minor element additions.

- Sulfur segregated to the exterior surfaces of samples heated in an Auger spectrometer and its concentration was reduced by yttrium additions and laser processing.

Accession For

NTIS GRA&I	☑
DTIC TAB	☐
Unannounced	☐
Justification	

By

Distribution/

Availability Codes

| Dist | Avail and/or Special |

A-1

1

R83-916154-1

A Study of Adherent Oxide Formation

TABLE OF CONTENTS

I. INTRODUCTION

All structural alloys are, with respect to high temperature oxidizing environments, thermodynamically unstable and react to form surface layers or scales. The composition, microstructure and performance characteristics, e.g. adherence of such scales, depends upon substrate chemistry and phase distribution as well as the service environment.

Improved oxide scale adherence through the the addition of low levels of reactive elements such as yttrium and hafnium has been repeatedly documented in the literature. Despite extensive research in this area, agreement on a single mechanism to account for the scale adherence benefits is lacking. Mechanisms proposed in the literature to account for these effects include:

1. formation of oxide pegs which anchor the scale to the substrate (Ref. 1);

2. prevention of vacancy coalescence and void formation at the scale-metal interface by providing alternate vacancy coalescence sites (Ref. 2);

3. enhancement of scale plasticity by altering the intrinsic mechanical properties of the oxide scale perhaps by the effect of fine reactive oxide particles at grain boundaries within the scale (Ref. 3);

4. modification of growth processes by interfering with normal transport mechanisms (Ref. 4);

5. formation of a graded oxide layer which better accommodates mechanical property differences between the protective scale and the substrate metal (Ref. 5).

It must be recognized that these mechanisms are not mutually exclusive. Moreover, enhanced scale adhesion effects from differing elements need not necessarily be the result of the same mechanism.

Recent experiments at UTRC have shown that laser melting and rapid solidification of thin surface layers on MCrAlY coatings improves oxide adherence over and above that observed for yttrium additions. Potential mechanisms for the improved adhesion due to laser-processing include microstructural refinement due to rapid solidification, purification of material by high superheats, redistribution of critical minor elements, and the formation of a thin oxide scale during laser processing which maintains adherence during subsequent oxidation.

The objective of this program is to characterize the effect(s) by which laser-processing and minor element additions improve oxide scale adherence of turbine coating compositions. This report presents progress during the first contract year. A NiCrAl coating composition has been selected and prepared with and without minor element additions. Surfaces have been subjected to laser-processing and the microstructural changes induced have been investigated. Isothermal and cyclic oxidation tests have been conducted and oxide scale structure, chemistry and adherence investigated. Techniques to heat samples within an Auger chamber and monitor surface chemistry have been developed and preliminary experiments performed.

II. EXPERIMENTAL MATERIALS AND PROCEDURES

A. Materials Preparation and Procedures

Alloys were prepared using nickel and aluminum of 99.9 w/o purity and chromium of 99.99 w/o purity. The proper elemental combinations were combined, vacuum melted in alumina crucibles, and poured into 2.5 cm chilled copper molds. Six rods (two each of Ni-20w/o Cr-12w/o Al, Ni-20w/o Cr-12w/o Al-1w/o Hf, and Ni-20w/o Cr-12w/o Al-0.1w/o Y) were prepared and homogenized by heat treating in vacuum at 1200°C for 48 hours to reduce solidification induced compositional gradients. Materials were analyzed for nickel, chromium, aluminum, yttrium and hafnium by x-ray fluorescence, and for sulfur and carbon by combustion using a Leco analyzer.

Disk shaped sections 6 mm thick were cut from the homogenized rods and polished through 600 grit SiC paper. After cleaning in absolute ethanol, two samples of each composition were laser melted on one surface using a 7 kW beam, 1.25 mm spot size, and 800 cm/min traverse speed. Overlapping passes were used to cover the disk surface. Disks were cut into 6 smaller samples as shown in Fig. 1. To avoid abrasion or contamination of the surface during cutting, the surfaces were coated with acetone soluble stop-off lacquer. Following cutting, the lacquer was dissolved in acetone.

The surface topography, structure, and chemistry of the polished and laser-processed surfaces were studied using optical and scanning electron microscopy. A cross section normal to the laser passes was metallographically prepared and etched with AG-21 solution (60% volume lactic acid, 37% nitric acid, 3% hydrofluoric acid). Observations were made of both the substrate and laser-processed materials using a combination of optical and scanning electron microscopy in conjunction with energy dispersive x-ray analysis. For oxidized samples, specimen surfaces were examined by optical and scanning electron microscopy using a carbon coating to effect electrical conductivity and thereby minimize charging.

B. Oxidation Studies

Specimens of NiCrAl, NiCrAlY and NiCrAlHf were cyclically and isothermally oxidized. Isothermal oxidation was performed in air at 1050°C for 100 hours. Cyclic oxidation testing was conducted in air at 1050°C with a one hour cycle (55 minutes at 1050°C and 5 minutes at room temperature) for 100 cycles. The environment for all oxidation experiments was stagnant laboratory air. For each test, three surface conditions were evaluated: 1) polished through 600 grit SiC,

3

2) laser-processed, and 3) laser-processed and polished with 600 grit SiC. The purpose of preparing the last surface condition was to determine if the thin oxide scales formed during laser-processing influenced oxide adherence.

C. Auger Studies

The primary objective of this year's Auger studies was to develop the equipment and techniques for in-situ heating to 1000°C and simultaneous Auger analysis of surface chemistry. In addition, preliminary experiments were conducted on samples of NiCrAl, laser-processed NiCrAl, and NiCrAlY.

Initial in-situ heating studies were conducted using a model 540 scanning Auger microprobe. Figure 2 shows the configuration of the specimen, sample heater, electron gun, cylindrical mirror analyzer, and ion sputter gun. The heater consisted of a resistance heated niobium wire filament surrounded by tantalum heat shields to which the specimen was clamped facing the electron beam and analyzer. A thermocouple placed in contact with the specimen was used to monitor temperature.

Two NiCrAl specimens were prepared by making a single laser pass on a polished longitudinal section of the rods. Rectangular specimens (1x1x0.1 cm) were then cut with the laser pass traversing one surface. The specimens were cleaned in absolute ethanol in preparation for Auger studies.

The following sequence of Auger procedures was used: a) evacuation of the chamber to a 10^{-9} torr, b) chamber backfill with argon and ion sputter etching (2 KV, 30 ma) to remove atmospheric surface contamination, c) chamber evacuation to ~ 10^{-9} torr, d) specimen heating and Auger analysis, e) chamber backfill with argon and ion sputter etching and Auger analysis to provide chemical depth profiling. Due to concerns that the scanning electron optics would be damaged by high temperature, most analysis was done after allowing the specimen to rapidly cool prior to positioning in front of the electron gun. In some instances simultaneous heating and analysis was performed and results were similar to those obtained after rapid sample cooling. Specimen temperatures were of 570°C, 700°C, and 780°C were investigated; the maximum temperature capability of the heater was found to be ~ 800°C.

A new heater design was implemented on a fixed beam Auger spectrometer to increase temperature capability to 1000°C and a second set of experiments was conducted on NiCrAl and NiCrAlY specimens. Figure 3 is a schematic of the Auger chamber, heater, electron gun and analyzer, ion gun, and argon and oxygen inlet valves. The sample was heated by conduction from a Kanthal (FeCrAl) strip which was heated by electrical resistance. Sample temperature was measured by means of

a thermocouple spot welded to a sample. The Auger procedures followed were identical to those used in the previous studies except that temperature was rapidly raised to 1000°C and analysis was conducted with the samples hot.

Estimated surface compositions were obtained from Auger spectra by measuring peak heights and using elemental sensitivity factors as discussed in the Handbook of Auger Spectroscopy (Ref. 6). Results are semiquantitative since this technique neglects variations in electron back scattering and escape depth.

III. RESULTS AND DISCUSSION

A. Materials

The chemical analysis of the cast rods are given in Table I. The concentrations of major alloying elements (chromium and aluminum) were near nominal compositions and no significant difference was noted between alloy type. The NiCrAl alloys contained yttrium and hafnium in concentrations below 0.01 w/o. The NiCrAlY samples contained 0.07-0.09 w/o yttrium and the NiCrAlHf samples contained 0.70-0.76 w/o hafnium; some minor losses occurred during casting. The carbon contents of all alloys were low (< 0.01 w/o). All six samples contained approximately 50 weight ppm sulfur as an impurity.

The laser melt zone depth (as determined from optical metallographic studies for all three alloy compositions) was approximately 100 μm. Materials within this zone was greatly refined by rapid solidification relative to the substrate microstructure (Fig. 4a). The substrate microstructure consisted of the nickel solid solution γ matrix, coarse β(NiAl) particles, and smaller precipitates within the β phase (Fig. 4b). The structure within the laser-processed material contained at least two phases resolvable by optical microscopy (Fig. 4c).

Scanning electron microscopy provided more detailed microstructural analysis (Figs. 5a through 5c). The substrate of all three alloys contained coarse aluminum rich β(NiAl) in a chromium rich γ matrix. At high magnification the fine particles dispersed within the β were found to be chromium-rich and appear to be the bcc α chromium phase, Fig. 6. Particles were also found dispersed within the γ which appear to be β, Fig. 6. Based upon their small size, it appears that the fine particles dispersed within both the coarse β and γ had been formed upon cooling since coarsening would have occurred rapidly at 1200°C. Thus at equilibrium at 1200°C the alloy apparently contains only two phases, γ and β.

The yttrium and hafnium doped samples contained additional phases. In the NiCrAlY, yttrium-rich particles approximately 2 μ in diameter were identified in the substrate as shown in Figs. 7a and 7b. The results of closer analysis of these particles is given in Figs. 8a through 8d. The oxygen x-ray map indicated an oxygen enrichment. However, an x-ray spectra suggested concentrations of nickel and chromium in addition to yttrium. Further analysis is required to determine whether the yttrium-containing particles were oxides and/or inter-metallic compounds.

For the NiCrAlHf, hafnium-rich particles approximately 2 μm in diameter were present in the substrate and were much more plentiful than the yttrium-rich

particles in NiCrAlY, (Figs. 9a through 9c). These particles were not oxides since no oxygen enrichment was observed. Analysis, which showed high concentrations of nickel and chromium in addition to hafnium, indicated the particles were intermetallic compounds (Figs. 9b and 9c). Some of the particles also showed traces of sulfur and zirconium suggesting that they had acted as getters for sulfur in the alloy (Fig. 9c).

For both NiCrAl and NiCrAlY, the laser-processed structure consisted of a matrix of γ containing β particles sizes in the range of 0.5-1 μm, (Fig. 10a). Other phases, if present, were beneath the resolution of the electron microprobe. The yttrium-rich phase in the substrate had been either eliminated or greatly refined. For NiCrAlHf, some large (2 μm) hafnium-rich particles were also present in the laser melted zone but they were much less numerous than in the substrate. Much finer particles ($<$ 0.25 μm) were also observed in the laser-processed zone and effected visual images similar to the large hafnium-rich particles (Fig. 10b). Laser processing had refined the hafnium-rich particles relative to the substrate.

A low magnification back scattered electron micrograph of the surface of laser-processed NiCrAl is given in Fig. 11. The NiCrAlY and NiCrAlHf alloys were similar in appearance. The overlapping laser passes were clearly evident with surface oxide or slag phases (which appear dark in backscattered electron images) along with the seam between passes. Such slags also appeared as rows of particles along paths of liquid metal flow. X-ray analysis showed that the slag particles contained high aluminum contents in all three alloys, Figs. 12a through 12c. Detectable concentrations of yttrium and hafnium were evident for NiCrAlY and NiCrAlHf alloys respectively. The slag nickel and chromium peaks may be due to contributions from the substrate. The morphology indicates the slag particles were formed during laser processing and swept by metal flow to the edge of the laser melted zone.

In addition to slag particles, high magnification micrographs (Fig. 13) indicated the presence of a continuous fine grained deposit on the laser melted surfaces. The very thin nature of this deposit precluded meaningful x-ray analysis. However, studies using Auger analysis reported in Section IIIC indicated that the surface of laser-processed NiCrAl was covered with aluminum oxide.

B. Oxidation Studies

1. NiCrAl

Polished Surfaces

In agreement with numerous prior studies, on thermal cycling--even on cooling to room temperature from an isothermal test--the protective scales formed

on the NiCrAl extensively exfoliated, Fig. 14. From the patches of scale locally retained, the oxide formed, about 2 μm thick, was highly wrinkled but relatively uniform in morphology, q.v. such was not the case for the oxidized NiCrAlY and NiCrAlHf alloys, Fig. 15. The oxide scales formed on the NiCrAl specimen were chiefly composed of large columnar grains, Fig. 15. The surface structure of the oxide suggested porosity the depth of which could not be established by simple surface examination, Fig. 16.

The metal surface below the oxide scale exhibited isolated features which could be construed as Kirkendall voids, Fig. 17. Although it has been proposed that Kirkendall porosity is a principle cause of scale exfoliation (Refs. 8 and 9), no extensive formation of Kirkendall porosity at the scale-metal interface was observed. The general facetting of the metal substrate as shown in Figs. 16 and 17 at the base of the oxide scale does not differ substantially from that found for similarly tested NiCrAlY and NiCrAlHf specimens upon which the oxide was very adherent.

Laser-Processed Surfaces

Oxide scale formed on the laser-processed NiCrAl specimen exfoliated as was the case from the non-laser-processed NiCrAl. Characteristically the oxides were similar in appearance to that observed for non-laser heated surfaces, Fig. 18, cf. Fig. 14. The oxide which formed was about 2 μm thick. Moreover gross oxide appendages at the metal-scale interface which would anchor or "peg" it to the substrate were not observed. Also, like the non-laser-processed surface, minimal Kirkendall porosity was observed in the metal surface just opposed to the exfoliated scales.

Laser-processed and abraded surfaces behaved similarly in oxidation to non-abraded surfaces, i.e., exfoliation of the oxide scale was the dominant effect. In cyclic oxidation, both as-annealed and laser-processed surfaces (regardless of whether they were abraded or not) exfoliated extensively to generate the less protective nickel and chromium-enriched oxides.

2. NiCrAlHf Specimens

Polished Surfaces

In contrast to the NiCrAl alloy, oxidized NiCrAlHf (and NiCrAlY) specimens showed distinctly different oxide morphologies over the β-NiAl dendrite islands

and the interconnected γ nickel solid solution, Fig. 19. Such a distinction was observed after both isothermal as well as cyclic testing. The oxide layer over the β-NiAl phase was thicker and exhibited apparently nodular crystals. The oxide layer over the γ solid solution phase was thinner with the final polish marks from the 600 grit SiC readily observed. Thus the presence of hafnium (or yttrium) in the alloy markedly affected the morphology of the oxide which grew on the surface of the alloy.

Superimposed upon this phenomena, hafnium-enriched oxides were present both in the oxides over the γ as well as the β phases. This is represented by the light areas in the back scattered electron micrographs, cf. Fig. 19 for the isothermal test results and Fig. 20 for the cyclic test results. Since the NiCrAl without any hafnium showed excessive scale exfoliation, the addition of hafnium markedly improved oxide scale adherence.

Laser-Processed Surfaces

For the laser-processed NiCrAlHf specimen, a more uniform oxide scale formed over the surface (disregarding the remnant lines of slag produced by the laser surface melting process itself), Fig. 21. The morphology of the oxide was similar to that found over the β-NiAl islands for the nonlaser-processed specimen. Energy dispersive x-ray analysis of this surface revealed enrichments of aluminum with low levels of nickel and chromium, Fig. 22. The nickel and chromium signals possibly resulted from the electron beam penetrating the thin oxide scales and sampling the underlying metal substrate. Only trace levels of hafnium were detected in the scale.

In some areas one oxide scale had locally ruptured at temperature leading to the formation of lesser protection nickel and chromium enriched scale with lower aluminum levels, Fig. 22 and 23. However the retained slag line was enriched in aluminum and hafnium with lesser amounts of nickel and chromium, Fig. 22.

Cyclic testing of the laser-processed NiCrAlHf optimum produced larger amounts of scale exfoliation to bare metal, Fig. 24. The laser-processed specimen which was abraded in order to remove the existing thin films also exhibited essentially a single morphology oxide microstructure as shown in Figs. 21 and 25. In cyclic tests, the scales formed on the as-processed and the abraded specimens spalled, Fig. 26. Moreover the morphology of the remnant oxide scale on the abraded and nonabraded surfaces was for all practical purposes identical. It is therefore concluded that the surface scale features are not due to the initial oxide formed during the laser processing treatment and are rather due to metallurgical/chemical effects produced by the laser.

Cyclic testing of the laser-processed NiCrAlHf specimen produced large numbers of scale exfoliated down to bare metal, cf. Fig. 24. Oxide pegs projected into the metal in regions where the scale had exfoliated, Fig. 27. Energy dispersive x-ray analysis of these "pegs" revealed hafnium-rich cores surrounded by an aluminum-rich phase. In areas where the oxide had been retained, oblique scanning electron microscopy examination failed to show evidence of marked peg development at the base of the scale. Thus it cannot be concluded that the coarse pegs markedly improved oxide adherence

3. NiCrAlY Specimens

Polished Surfaces

The as-annealed NiCrAlY specimens after 100 hours of isothermal testing at 1050°C exhibited a bimodal oxide morphology, Fig. 28. This was similar to that seen for the NiCrAlHf specimen but markedly different from that shown by NiCrAl. The oxide over the β-NiAl phase was thicker than that over the γ solid solution phase. However unlike NiCrAlHf which exhibited blocky nodular growths, the enhanced oxide growths over the β-NiAl precipitates in the NiCrAlY were charac-terized by crystallites more platelike in microstructure, cf. Fig. 28. Differ-ences in the gross oxide morphologies of scales formed over oxidized NiCrAlY alloys have been previously reported (Ref. 10). However a detailed characteriza-tion of such differences in oxide microstructure has been lacking. For the sake of completeness, an additional minor effect was also noted. Locally enhanced oxide growth over residual scratches derived from the specimen polishing opera-tion was noted even over the γ phase. It is well known that abraded surfaces can produce enhanced diffusion effects leading to transient, localized, increased oxidation kinetics. This effect was also observed for the NiCrAlHf specimens.-

The oxide scale formed on the NiCrAlY specimen was very adherent. This was markedly better than that found for the NiCrAlHf alloy tested here and infinitely better than that observed for the NiCrAl alloy lacking either hafnium or yttrium. Similar adhesion characteristics were observed for oxides scales on NiCrAlY after thermal cycling.

In the non-laser-treated surfaces, a distinct difference in the yttrium distribution in oxide scales was found dependent upon whether the test was conducted isothermally or cyclically. In isothermal tests, isolated islands of yttrium-enriched oxides were randomly distributed in the oxide scales across both the γ nickel solid solution and the β-NiAl phases, e.g. Fig. 29. Energy disper-sive x-ray analysis of the bright areas in the back scattered electron micro-graphs affirmed localized yttrium enrichments in such regions. On the other hand, for the cyclically tested specimens, a marked increase occurred in the

quantity of yttrium-rich particles found both in the thicker oxides overlying the β-NiAl phase as well as at the interface between the β-NiAl and γ solid solution phases, Fig. 30 cf. Fig. 29. In the thermally cycled specimen, qualitatively fewer segragated yttrium-enriched oxide particles occurred in the oxide over the γ.

A diamond scribe was used to abrade the oxidized surface of the isothermally tested specimen in order to characterize the scale in cross section without the complications associated with mounting and polishing or chemically etching the specimen. It is interesting to note that the cracks produced in the abrasion path were suggestive of plastic flow in the oxide layer, Fig. 31. Scale spalla-tion was restricted to the scale immediately adjacent to the scribe paths, Fig. 31.

An examination of the retained scale adjacent to areas of exfoliation revealed a multi-layered alumina oxide scale, Fig. 32. Over the γ, a three zone oxide layer was observed. The outermost layer which appeared flat in surface observation was about 0.1 μm thick, Fig. 32. Below this layer a fine grained porous appearing zone was observed, Fig. 32. Immediately adjacent to this and extending to the metal substrate below, was a relatively large grained apparently columnar oxide, approximately 1.5 μm thick, Fig. 32. At the base of the oxide, fracture had occured within the scale itself. The interfacial region immediately between the oxide and the scale was not marked by large amounts of voids. However below such exfoliated regions occasional microporosity in the metal at the metal-scale interface was encountered, Fig. 33. Such microporosity was either due to Kirkendall effects or the result of micropegs being pulled out when the scale locally exfoliated.

Regarding the oxide layer over the β-NiAl, a two zone oxide layer occurred, Fig. 34. An outer layer of nodular oxide growth which visually appeared porous had grown to a thickness of about 2.8 μm. Below this layer, a zone of large grained columnar oxide, about 1.5 μm thick, had developed. The thickness of the columnar grained layer in contact with the metal was the same regardless of whether it was formed over the γ or the β phase.

The areas of the NiCrAlY from which scales exfoliated due to abrasion did not show evidence of large numbers of yttrium-rich oxide pegs adherent to the underlying metal. However it would be erroneous to say that no such features existed. Extensive searching of many such exfoliated regions did reveal a few such features, Fig. 35. However they were very few in number and certainly not microstructurally obvious. This observation contrasted with that noted for the comparably tested NiCrAlHf alloy, cf. Fig. 28.

Lastly, based upon scanning electron microscope analysis of the surface produced by diamond scribing, the metal at the base of the oxide scale appeared to be covered by a very thin, transparent, glassy or almost amorphous-appearing film, Fig. 35. Neither very high resolution scanning electron microscopy nor prolonged examination by energy dispersive x-ray analyses could adequately characterize the nature of the film.

Laser-Processed Surfaces

After isothermal testing, the laser-processed surface exhibited a markedly different oxide structure than that observed over the as-annealed NiCrAlY specimen, Fig. 35. The oxide was adherent and at lower magnifications visually looked similar to the oxide structure over the β-NiAl phase in the as-annealed test specimen condition. Higher magnification examination affirmed the relatively uniform texture of the scale produced, Figs. 36 and 37. However the surface microstructure of the laser-processed surfaces differed in detail from that found over the β phase in the as-annealed specimen condition, Fig. 37. The oxide surface was characterized by a plethora of tubular or whisker-like (presumably alumina) oxide growths on what appeared to be a porous surface layer as opposed to what were almost plate-like growths over the β precipitates for the non-laser-processed specimen. This morphology was unique and was not observed on any of the other specimens.

In prior studies, the development of alumina whiskers on alumina formers was associated with the presence of trace levels of gaseous corrodents such as NaCl in the test atmosphere (Ref. 7). However it is unclear why one series of alloys, i.e., the laser-processed NiCrAlY alloy, was prone to such whisker development when the other alloys were not, even when all the alloy test coupons were tested side by side.

Except for the yttrium obviously present in the oxide slag regions, energy dispersive x-ray techniques failed to reveal the presence of yttrium above background levels in the uniform oxide scale, Fig. 38. This does not mean that the yttrium content in the alloy was uniquely zero. It simply means that the yttrium present in the oxide layers was below that detectable by energy dispersive techniques.

Regarding the yttrium present in these oxide scales, two observations are noteworthy. In the first place, obviously the yttrium distribution in the oxide scale over the laser-processed surface differed markedly from that seen for the as-annealed NiCrAlY specimens after either isothermal or cyclic testing. In the second place, although the yttrium present in the oxide of the laser-processed then isothermally tested specimen was very low (below detectability limits for energy dispersive x-ray techniques), its presence - even at this low level - was

12

necessary to promote oxide scale adherence. Recall that the laser-processed NiCrAl with no yttrium produced great amounts of scale exfoliation even upon cooling from an isothermal test.

Diamond scribing the isothermally tested laser-processed NiCrAlY specimen revealed that the retained oxide scale had formed large numbers of alumina whisker-like growths on its surface, Fig. 39 cf. Fig. 37. In areas where the retained oxide scale had partially lifted from the metal, no indication of any gross oxide pegs which would serve as scale attachment points to the underlying metal were observed, Fig. 39.

The oxide structure produced here exhibited two layers. The outermost layer which included the prominant alumina whiskers was about 2.5 μm thick and was obviously porous, Fig. 40. The innermost layer was approximately 0.5 μm thick and was essentially comprised of small equiaxed grains, Fig. 40. In contrast the oxidized as-annealed NiCrAlY specimen similarly tested showed a thick zone, about 1.5 μm thick, of columnar grains adjacent to the metal, cf. Figs. 32 and 34. Although the interface between the oxide scale and the substrate metal was characterized by considerable microporosity (Fig. 40), the scale was strongly adherent. Such microporosity contrasted with that observed for the as-annealed NiCrAlY specimen similarly tested, Fig. 32.

An experiment was conducted to determine if the differences in oxide struc-ture between the as-annealed and laser-processed surface resulted largely from a coarsening of the thin oxide layer produced in the laser surface melting process. A laser-processed NiCrAlY surface was mechanically abraded with 600 grit SiC polishing paper to remove this initial oxide layer prior to oxidation. After high temperature isothermal testing, the oxide produced was found to be morpholo-gically uniform, Fig. 41, appearing very similar to that observed on the laser-processed but not mechanically abraded surface. Additionally, as previously no yttrium was found above background levels in the adherent oxide scale. Because of these similarities in oxide microstructures and yttrium distribution for the laser processed NiCrAlY specimens (irrespective of whether they are abraded or not) and the great differences with the as-annealed NiCrAlY test results, it was concluded that the uniform oxide produced was not due to the initial thin oxide layer formed in the laser process. Rather the difference in oxide morphology intrinsically resulted from the chemical/metallurgical effects incurred during the laser processing. The observations made as a result of tests conducted with laser-processed NiCrAl and NiCrAlHf alloys were in agreement in this regard.

4. Important Observations

● Laser surface processing altered oxidation processes. Specifically the laser-processed NiCrAlY specimens behaved significantly different in both

13

the isothermal and cyclic 1050°C test when compared with the non-laser-processed alloys of the same composition. Uniform and thinner dense oxide layers were associated with laser processed test specimens.

- The effects of laser processing were not due to the initial oxide scales produced during laser processing. Laser-processed specimens which were mechanically abraded prior to testing performed similarly to specimens which had not been abraded.

- The effects of laser processing on oxide scale development were not due to an inversion of the relative amounts of the major phases present in the NiCrAlHf and NiCrAlY compositions. Both before and after laser surface processing, the γ nickel solid solution phase was the continuous phase with isolated islands of β-NiAl distributed in it.

- From the viewpoint of oxide scale adherence, the major effect was attributed to yttrium. Its presence, even at levels too low to be detectable by energy dispersive x-ray techniques, was crucial. Laser-processed NiCrAlY, which exhibited no yttrium in oxide scales above background levels, performed immeasurably better than NiCrAl.

- Hafnium was not as effective as yttrium in promoting oxide scale adherence. The hafnium contents in the alloys here were about 0.2 a/o while the yttrium contents were about 0.05 a/o. The presence of hafnium even at the 0.2 a/o affected better oxidation resistance than the NiCrAl alloy alone.

- Yttrium distributions in the oxide scale depended upon test condition. Isothermal testing resulted in yttrium-rich oxide blooms randomly distributed in the scale above the γ and β phases. Cyclic testing resulted in a marked increase in the segregation of the yttrium to the oxide scale above the β phase and above the interface between the γ and β phases.

- Based on residual oxide fragments, apparently uniform oxide scales form over NiCrAl. However complex alumina scales develop over NiCrAlY. For NiCrAlY specimens tested in the annealed condition, oxide layers over the γ phase were three layered. Over the β phase, oxide scales were composed of two layers. In laser-processed NiCrAlY specimens, two layered scales were formed with whisker-like alumina formation in the outermost layer.-

- For the NiCrAl specimen, sufficient amounts of Kirkendall porosity were not found at the scale-metal interface to account for the poor scale adhesion observed.

● For NiCrAlY, a very few small pegs enriched in yttrium and pores in the
  metal were found at the scale-metal interface.

C. Auger Studies

Equipment and techniques were developed which allowed simultaneous heating
of the specimens to 1000°C and Auger analysis of surface chemistry (Fig. 3). The
Auger analysis results for the three sample types analyzed (NiCrAl, laser-
processed NiCrAl, and NiCrAlY) and both Auger systems were combined and are
tabulated in Tables II through VI. These results were obtained during equipment
and technique development studies and more systematic studies are planned.
However, information on minor element effects and laser processing were obtained
from analyzing the present results.

Table II presents the results of analysis of unheated sputter-cleaned
polished surfaces of NiCrAl and NiCrAlY; reasonably consistent results were
obtained for the four samples. Figure 42 is the Auger spectrum for NiCrAl.
Besides the alloying elements (nickel, chromium, and aluminum), high levels of
oxygen (~ 50%) and carbon (~ 10%) were observed. These two elements are common
vacuum chamber constituents which adsorbed on the sample surface following
sputtering. Low levels of sulfur (~ 0.5%) were also observed which represented
sulfur contamination from handling which was located in topographical areas
inaccessible to the ion beam. Sulfur is not a common vacuum chamber gas
contaminant. Not surprisingly, sputtered polished surfaces of NiCrAlY gave
similar results to the NiCrAl; the yttrium concentration was far below
detectable limits.

The surface compositions of NiCrAl induced by heating to 570°C, 700°C, and
1000°C are given in Table III. For 570°C and 700°C, the only significant change
in composition was an increase in sulfur concentration to 3% at 570°C and 7% at
700°C. Figure 43 is an Auger spectrum for NiCrAl at 700°C. The trend of
increasing sulfur with increasing temperature continued at 1000°C were a concen-
tration of 22% was present, Fig. 44. Additionally, carbon was completely
desorbed from the surface and oxygen concentration decreased dramatically to 4%
at 1000°C. High sulfur concentrations were removed from the specimen surfaces by
very brief sputtering indicating very strong segregation to the specimen
surface.

The results of analysis of laser-processed NiCrAl at 570°C and 700°C are
given in Table IV. Comparison of the as-sputtered composition to that for
sputtered polished surfaces (Table II) showed that laser-processing had greatly
reduced nickel and chromium concentrations and increased the aluminum concentra-
tion (14% to 37%); compare Fig. 45, an Auger spectrum of laser-processed to
NiCrAl to Fig. 42, a spectrum for non-laser-processed NiCrAl. SEM micrographs of

this surface (Fig. 13a) had shown a fine-grained surface deposit. The present results indicate that this deposit was aluminum oxide which formed when the metal was molten and aluminum had sufficient mobility to move to the exterior surface and react with oxygen present in the helium cover gas. Results in Section IIIB showed that this surface film and similar films on NiCrAlY and NiCrAlHf had little influence on oxidation or scale adherence. Heating this sample to 570°C and 700°C caused only minor chemistry changes with the most significant change being an increase in sulfur content to 2% at 700°C, Fig 46. This level was much lower than observed on non-laser-processed material at 700°C (7%). The chromium concentration was also much lower on this surface at 700°C than on the non-laser processed sample (3% vs. 15%).

Table V presents the results for a laser-processed sample which had been mechanically abraded. The composition of the sputtered surface was very similar to the polished non-laser-processed surface (Table II) indicating that the laser-process-formed aluminum oxide film had been removed. Results are presented for analysis conducted both before and after cooling. Heating caused very little change in surface composition with the exception of an increase in sulfur content to ~ 3% at 700°C and ~ 8% at 780°C. Note that the sulfur concentration at 700°C (2 to 3%) was significantly lower than that for non-laser-processed material (7%) but about the same as that for the laser-processed material with laser-formed oxide film intact (2%).

Heating the NiCrAlY sample to 1000°C (Table VI) caused a dramatic decrease in oxygen concentration (38% to 11%) and carbon concentration (17% to 0%) and an increase in sulfur content from 0% to 6%. The sulfur concentration was much lower than for the NiCrAl sample at 1000°C (6% vs. 22%). Compare Fig. 46 an Auger spectrum for NiCrAl at 1000°C to Fig. 47, an Auger spectrum for NiCrAlY at 1000°C.

Two general observations deserve further discussion, a) the segregation of sulfur to the sample surfaces and b) the lack of aluminum oxide scale formation during heating to temperatures as high as 1000°C.

While sulfur segregation cannot be directly related to oxide film adherence to the substrate; it is reasonable to suggest that similar enrichments occur at other interfaces, in particular the oxide-metal interface during oxidation in air. Sulfur is a notorious embrittler of interfaces, and its presence at grain boundaries in nickel and nickel base alloys renders the material susceptible to intergranular fracture (Refs. 11 and 12). The presence of sulfur at the metal-oxide interface could embrittle it and thereby produce more extensive spallation. The surface sulfur concentration was decreased by both yttrium additions and by laser processing. Similar reductions in sulfur at the metal-oxide interfaces due to yttrium additions and laser processing would explain the observed increase in

oxide adherence. Yttrium could reduce surface sulfur concentration by forming sulfides thereby reducing the concentration of sulfur available to segregate. Similar reductions in grain boundary sulfur level have been observed in nickel base alloys and have been attributed to this gettering mechanism (Ref. 13). Laser procesing may reduce sulfur segregation by either reducing bulk concentrations via exposure to high temperatures or it may provide small internal yttrium intermetallic particles or oxides which effectively getter sulfur.

It was initially thought that heating specimens in the intrinsic environment of the Auger vacuum chamber would result in continuous aluminum oxide film formation. Results, which show continuing high concentrations of nickel, chromium, and sulfur and very low oxygen concentrations at 1000°C, indicate continuous aluminum oxide scale formation did not occur. Since aluminum oxide scales form readily in air at these temperatures, the chamber environment must contain insufficient oxygen to allow significant oxide films to kinetically grow. Further, it is speculated that a reaction between segregated sulfur and absorbed oxygen may result in the formation of gaseous SO_2 thereby interfering with surface oxide formation. During experiments at 800°C, the delivery of sulfur to the surface was less rapid than at 1000°C allowing more oxygen absorption. The higher oxygen level which was observed on the NiCrAlY sample (11%) than on the NiCrAl sample (4%) at 1000°C also agrees with this hypothesis since the NiCrAl sample had much higher surface sulfur concentrations. A similar reaction between sulfur segregated to nickel surfaces and atmospheric oxygen has been documented several times (Refs. 14 and 15). A more plentiful supply of oxygen to the surface should overwhelm the segregating sulfur and enhance oxide scale formation. Therefore, provisions have been made to backfill the vacuum chamber to ~ 10^{-7} torr with oxygen gas (Fig. 3) and it has been demonstrated that simultaneous heating and analysis can be performed in this environment. This capability will be used in future studies.

IV. PROGRAM STATUS

Considerable progress has been made during this year in determining the effect(s) for improved oxide adherence through minor elements and laser processing. Materials (NiCrAl, NiCrAlHf, NiCrAlY) have been prepared, laser-processed, and chemically and microstructurally characterized. Isothermal and cyclic oxidation tests have been conducted and results analyzed in terms of oxide scale growth, structure, and chemistry. Experimental techniques have been developed and used to directly study surface chemistry during in-situ heating using Auger electron spectroscopy.

The five prominant mechanisms for improved oxide scale adherence through minor element additions were listed in Section I. Results presented and discussed in Section IIIB have shown that two of the commonly sited mechanisms (formations of pegs and prevention of void formation at the oxide scale inter- face) were not responsible for the improved oxide adherence in these materials through minor elements additions and laser processing. Auger studies in Section IIIC (which demonstrated sulfur segregation to the metal surfaces and that yttrium additions and laser processing reduced this segregation) lead to the proposition of an alternate explanation for oxide scale adherence improvement. According to this mechanism, minor elements and laser processing reduce sulfur accumulation at the oxide-metal interface thereby increasing interface strength.

In reference to the influence of laser processing on oxide adherence. It has been shown the oxide films formed on surfaces during laser melting are not responsible for subsequent improved oxide adherence. Furthermore, improvements in oxide adherence require that the minor elements (in particular yttrium) are present during laser processing. Therefore, refinement of the microstructure in NiCrAl as opposed to NiCrAlY and NiCrAlHf by laser processing did not improve adherence. Two remaining mechanisms which were proposed in Section I for the influence of laser processing on oxide adhesion (redistribution of critical minor elements and purification of the metal due to high superheat) need further inves- tigation.

V.   FUTURE RESEARCH

Based upon the results of this study efforts will be directed as follows:

1) The influence of minor element additions (yttrium and hafnium) and laser processing on oxide adherence will be quantified from isothermal and cyclic oxidation tests.

2) Detailed microstructural analysis will be conducted to determine the effect(s) responsible for oxide adherence. These include the influence of laser processing on (a) minor element distribution and form in the metal (b) the chemistry and structure of the oxide – metal interface and (c) the chemistry and structure of the oxide scale.

3) Systematic in-situ Auger heating experiments will be conducted to quantify the influence of laser processing and minor elements on sulfur segregation. Oxidation will be studied by back filling the chamber with oxygen during heating.

VI. ACKNOWLEDGEMENTS

20

VII. REFERENCES

1. Whittle, D. P. and J. Stringer; _Phil. Trans. Royal Soc._, London A295, p. 309 (1980).

2. Tien, J. K. and F. S. Pettit: _Metall Trans._, 3, pp. 1587-1599 (1972).

3. (a) Antill, J. E. and K. A. Peakall: _J. Iron and Steel Inst._, 205, pp. 1136-1142 (1967).
    (b) Francis, J. M. and J. A. Jutson: _Corros. Sci._, 8, pp. 445-449 (1968).

4. Golightly, F. A., F. H. Stott, and G. C. Wood: _Oxid. of Metals_, 10, pp. 163-187 (1976).

5. Pfeiffer, H.: _Werkst. Korros._, Mannheim, 8, p. 574 (1957).

6. Davis, L. E., N. C. McDonald, P. W. Palmberg, G. E. Raich, and R. E. Weber: _Handbook of Auger Electron Spectroscopy, Physical Electronics Industries_, Eden Prarie, MN, p. 5, 1976.

7. Smeggil, J. G. and N. S. Bornsetin: Study of the Effects of Gaseous Environments on the Hot Corrosion Resistance of Superalloy Materials, NASA CR-159747, January 1980.

8. Giggins, C. S. and F. S. Pettit: Oxide Scale Adherence Mechanisms and the Effects of Yttrium Oxide Particles and Externally Applied Loads on the Oxidation of NiCrAl and CoCrAl Alloys, ARL-TR-75-0234, June 1975.

9. Allam, I. M., D. P. Whittle and J. Stringer: _Oxid. of Met._ 12, pp. 35-66 (1978).

10. Reddy, K. P. R., J. L. Smialek and A. R. Cooper: _Oxid. of Met._ 17, pp. 424-448 (1982).

11. Johnson, W. C., J. E. Doherty, B. H. Kear, and A. F. Giamei: _Scripta Met._ 8, p. 971, 1974.

12. Doherty, J. E., A. F. Giamei, and B. H. Kear: _Can. Met. Quart._, 13, p. 229, 1974.

13. Mulford, R. A.: Met. Trans. A, 14A, p. 865, 1983.

14. Holloway, P. H., and J. B. Hudson: Surf. Sci,. 33, pp. 56-68, 1972.

15. Harris, L. A.: J. Appl. Phys., 39, pp. 1428-1431, 1968.

TABLE I

BULK ALLOY CHEMISTRY
(Weight %)

	Alloy	Cr	Al	Y	Hf	C	S
1)	NiCrAl	18.7	12.5	< 0.01	< 0.01	< 0.01	
2)	NiCrAl	19.6	12.6	< 0.01	< 0.01	< 0.01	0.006
3)	NiCrAlY	18.9	12.7	0.09	< 0.01	< 0.01	
4)	NiCrAlY	19.4	12.8	0.07	< 0.01	< 0.01	0.005
5)	NiCrAlHf	19.2	11.8	< 0.01	0.76	< 0.01	
6)	NiCrAlHf	19.1	12.8	< 0.01	0.70	< 0.01	0.004

TABLE II

ESTIMATED SURFACE COMPOSITION OF SPUTTERED
POLISHED SURFACES
(Atomic %)

	NiCrAl	NiCrAl	NiCrAl	NiCrAlY
Ni	15	16	28	27
Cr	10	13	7	4
Al	9	21	11	13
O	52	47	35	38
C	13	4	18	17
S	1	0	0.5	0

TABLE III

ESTIMATED SURFACE COMPOSITION OF HEATED NiCrAl
(Polished Surfaces)
(Atomic %)

	Sputtered[1]	570°C[2]	700°C[3]	1000°C[4]
Ni	20	14	12	35
Cr	10	14	15	14
Al	14	11	16	24
O	45	50	34	4
C	12	8	11	0
S	0.5	3	7	22

[1] Average of 3 samples (Table I)
[2] Heated and cooled
[3] Average of 2 samples, 1 hot and 1 heated and cooled
[4] Analyzed hot

TABLE IV

ESTIMATED SURFACE COMPOSITION OF HEATED LASER-PROCESSED NiCrAl
(Atomic %)

	Sputtered[1]	570°C	700°C[2]
Ni	5	4	10
Cr	2	0	3
Al	37	35	25
O	52	49	51
C	4	11	8
S	0	0.5	2

[1] Average of 2 samples
[2] Average of 2, 1 hot and 1 heated and cooled

TABLE V

ESTIMATED SURFACE COMPOSITION FOR
LASER-PROCESSED AND ABRADED SURFACES
(Atomic %)

	Sputtered	700°C (hot)	700°C (cold)	780°C (hot)	780°C (cold)
Ni	30	27	20	21	22
Cr	9	10	6	14	12
Al	14	24	25	20	22
O	37	31	40	32	37
C	10	6	7	4	4
S	0	3	2	8	7

TABLE VI

ESTIMATED SURFACE COMPOSITION OF HEATED NiCrAlY
(Atomic %)

	Sputtered	1000°C
Ni	27	42
Cr	4	13
Al	13	28
O	38	11
C	17	0
S	0	6
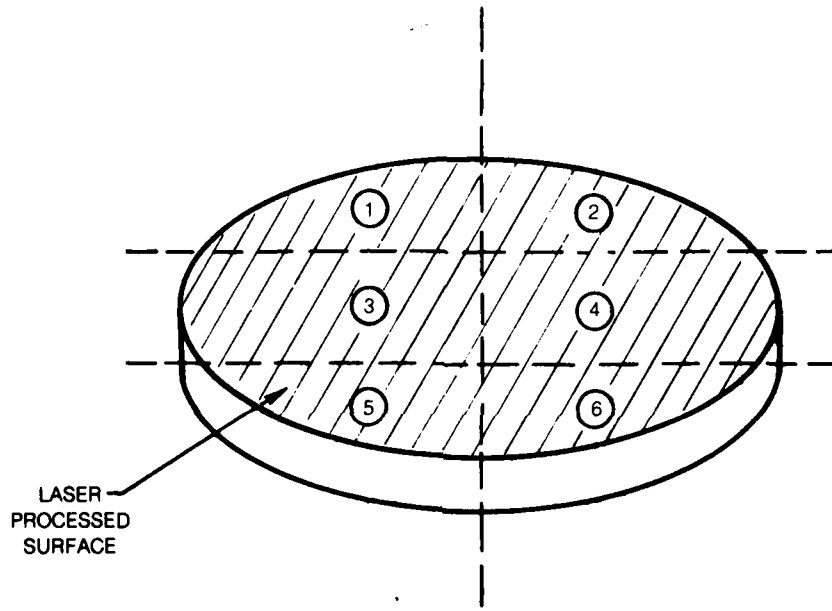
Figure 1. Sectioning Procedure for Laser-Processed Sample Disks

83-5-62-1
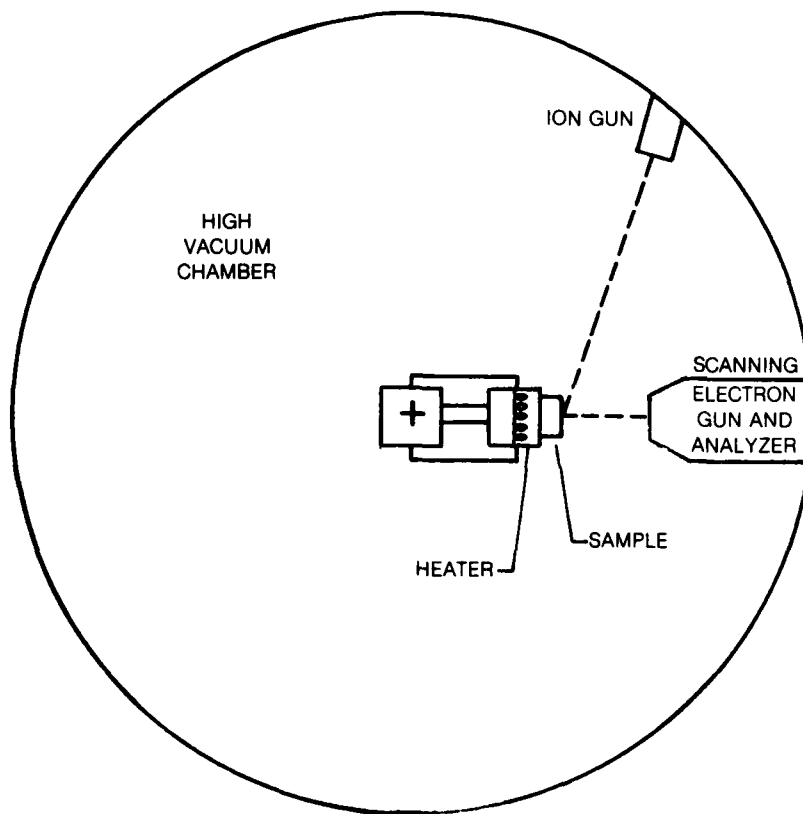
Figure 2. Scanning Auger Spectrometer and Sample Heater Used in Initial In-Situ Heating Experiments

83-1-100-4
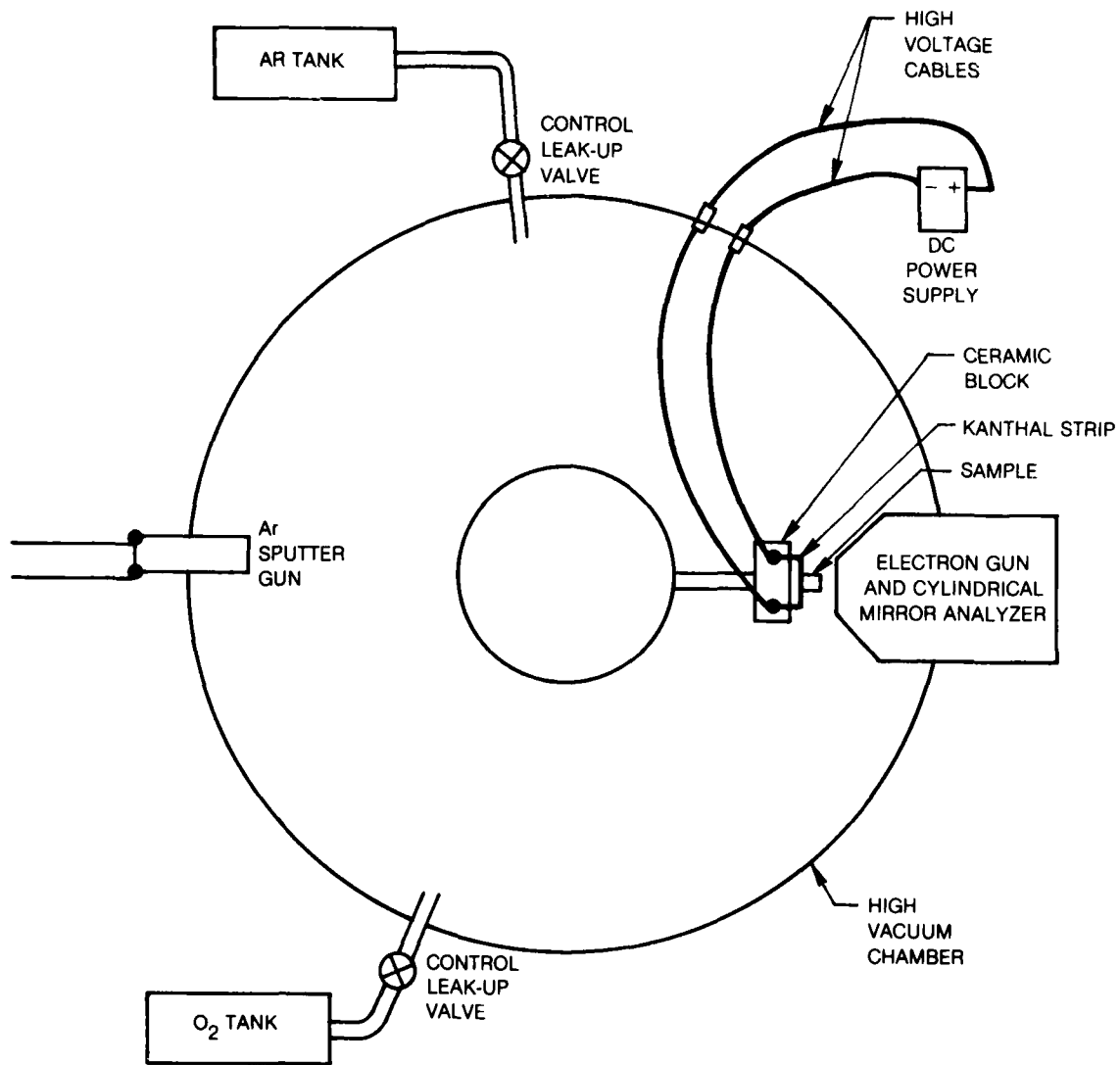
Figure 3. Auger System Equiped for Sample Heating to 1000°C, Controlled O$_2$ Additions, and Ar Ion Sputtering

83-10-11-1
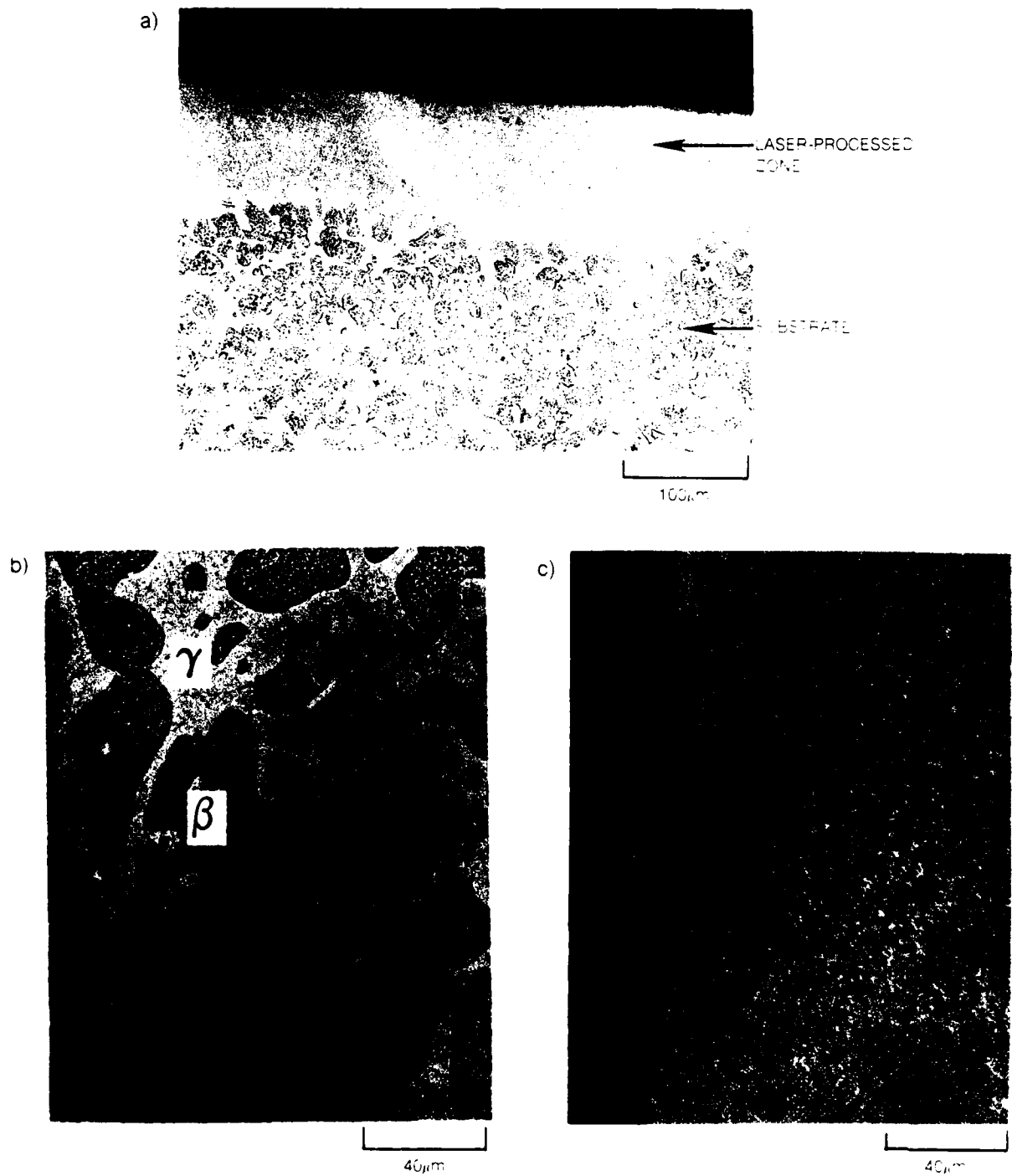
Figure 4. Optical Micrographs of Laser-Processed NiCrAl
   a) Overall View
   b) Substrate
   c) Laser-Processed Zone
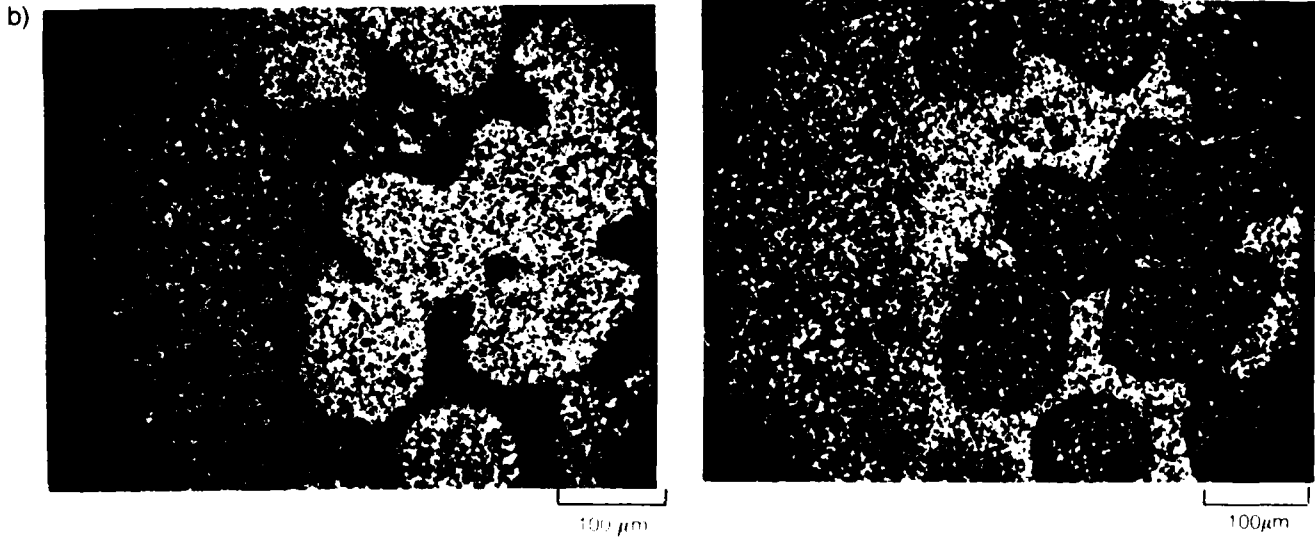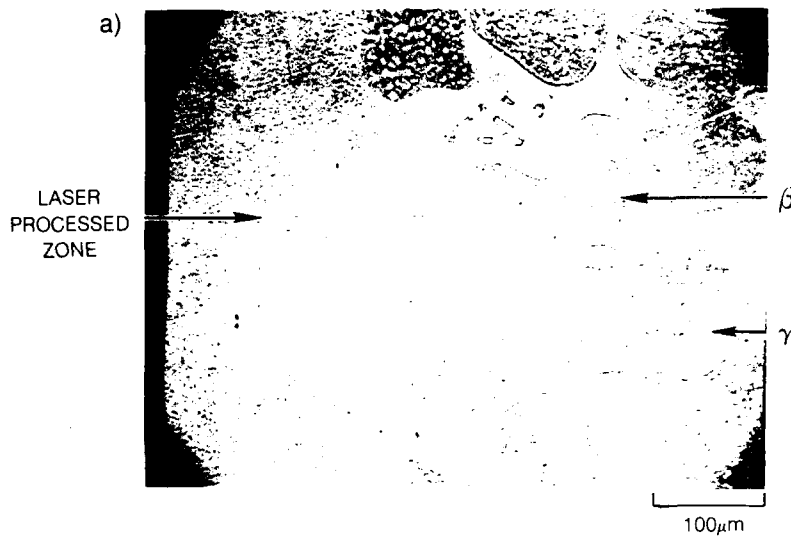
Figure 5. Electron Microprobe Studies of Laser-Processed NiCrAl
a) Electron Micrograph (SEM)
b) Aluminum X-ray Map
c) Chromium X-ray Map
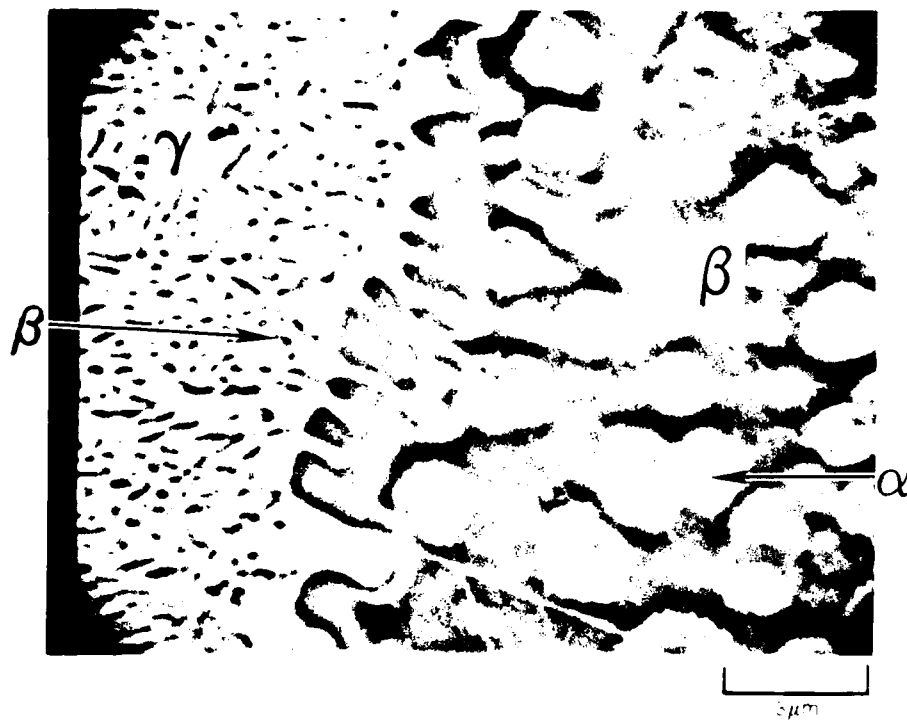
Figure 6. High Magnification Electron Micrograph (SEM) Showing Fine
β within γ and α within β in the Substrate Material.
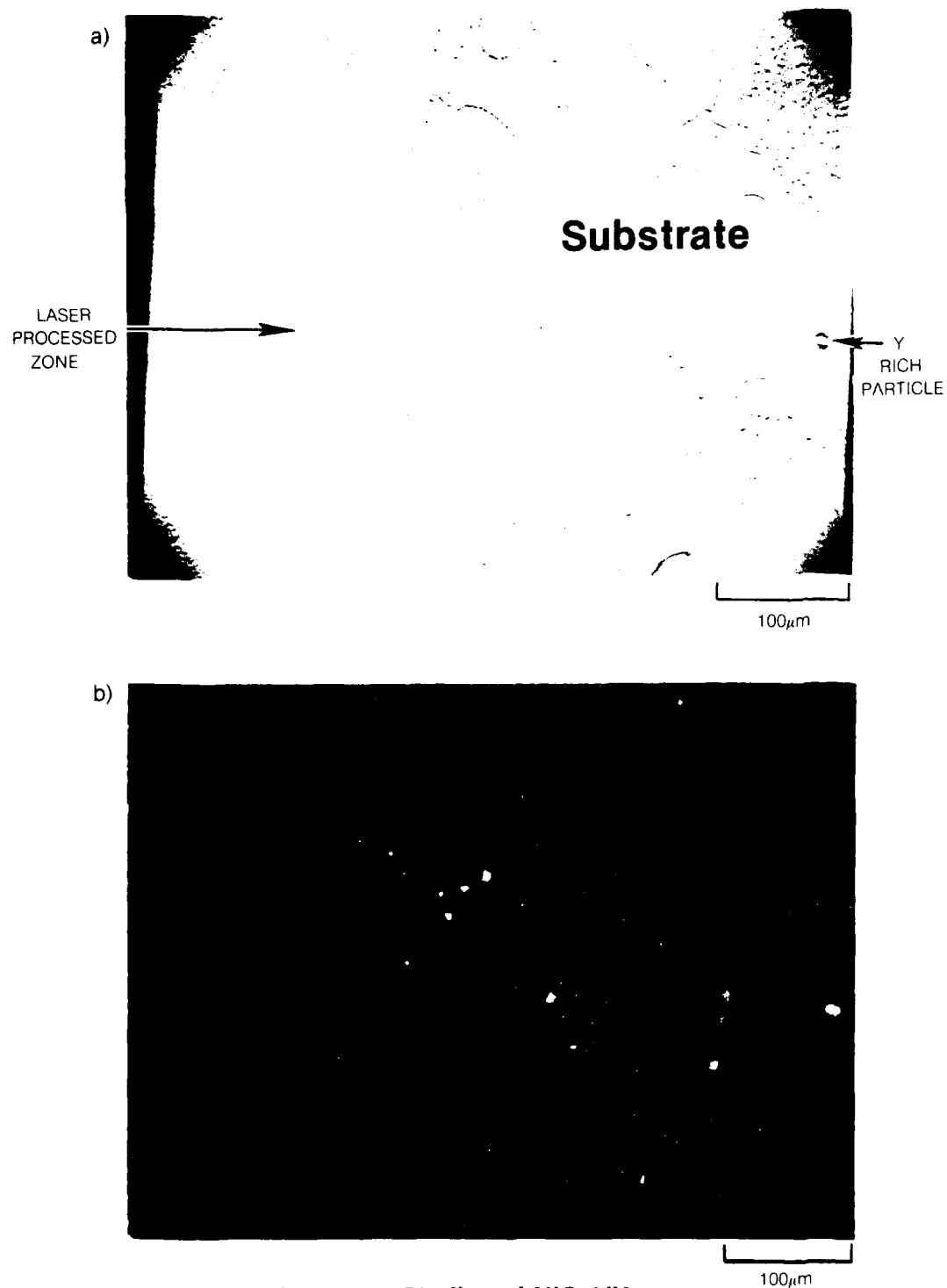
Figure 7. Electron Microprobe Studies of NiCrAlY
   a) Backscattered Electron Image Showing Laser-Processed Zone,
      Substrate, Yttrium Rich Particles in Substrate
   b) Yttrium X-ray Map
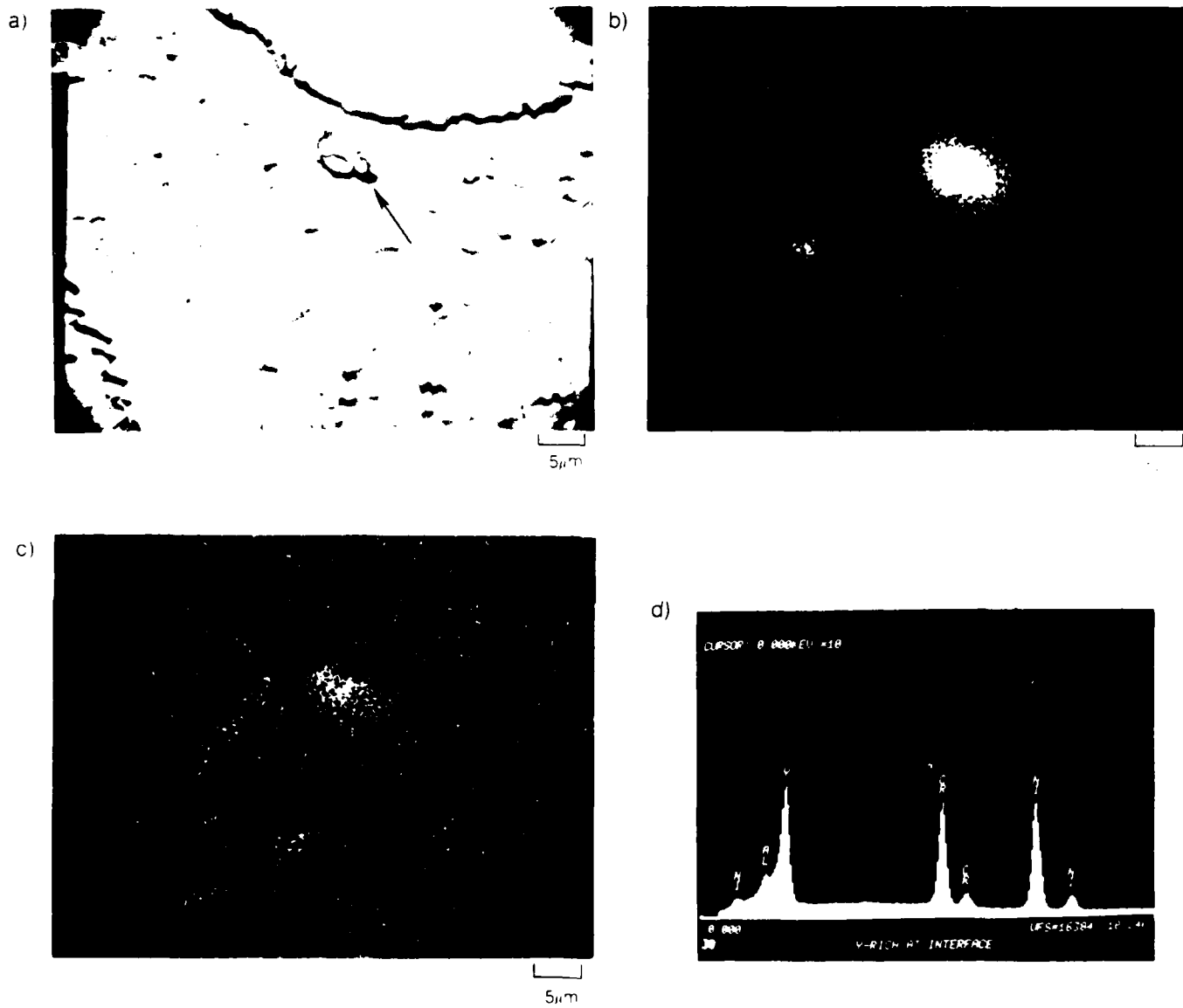
Figure 8. Electron Microprobe Studies of Substrate NiCrAlY
a) Backscatter Electron Image of Yttrium-Rich Particle
b) Yttrium X-ray map
c) Oxygen X-ray Map
d) X-ray Spectrum

a)

LASER
PROCESSED
ZONE

Hf RICH
PARTICLES

100μm

b)

c)
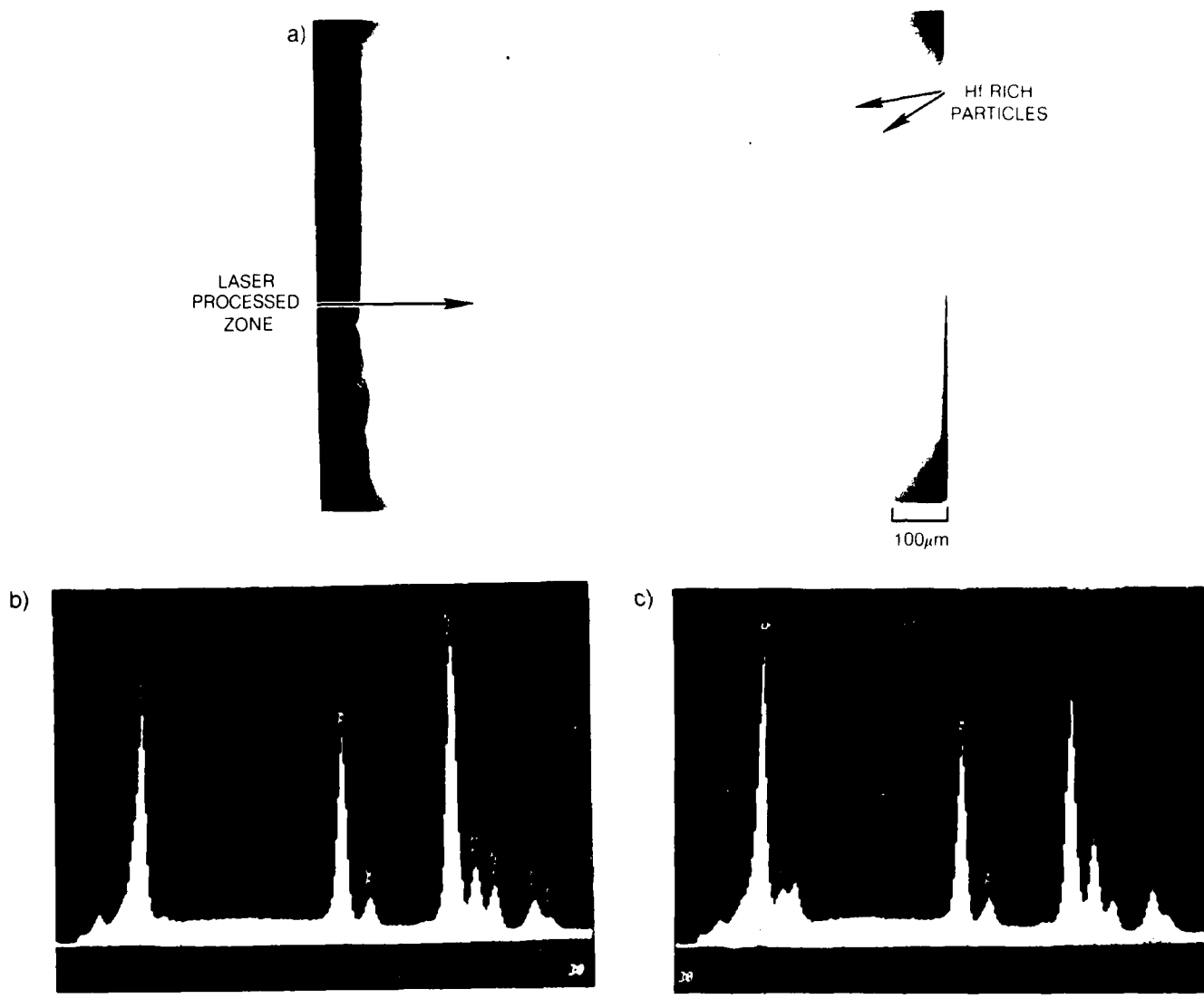
Figure 9. Electron Microprobe Studies of NiCrAlHf
    a) Backscatted Electron Image Showing Structure Refinement in Laser-Processed
       Zone and Hafnium Rich Particle in Substrate (White)
    b) X-ray Spectrum of one Hafnium Rich Particle Type
    c) X-ray Spectrum of the Second Hafnium Rich Particle Type

83-10-11-3
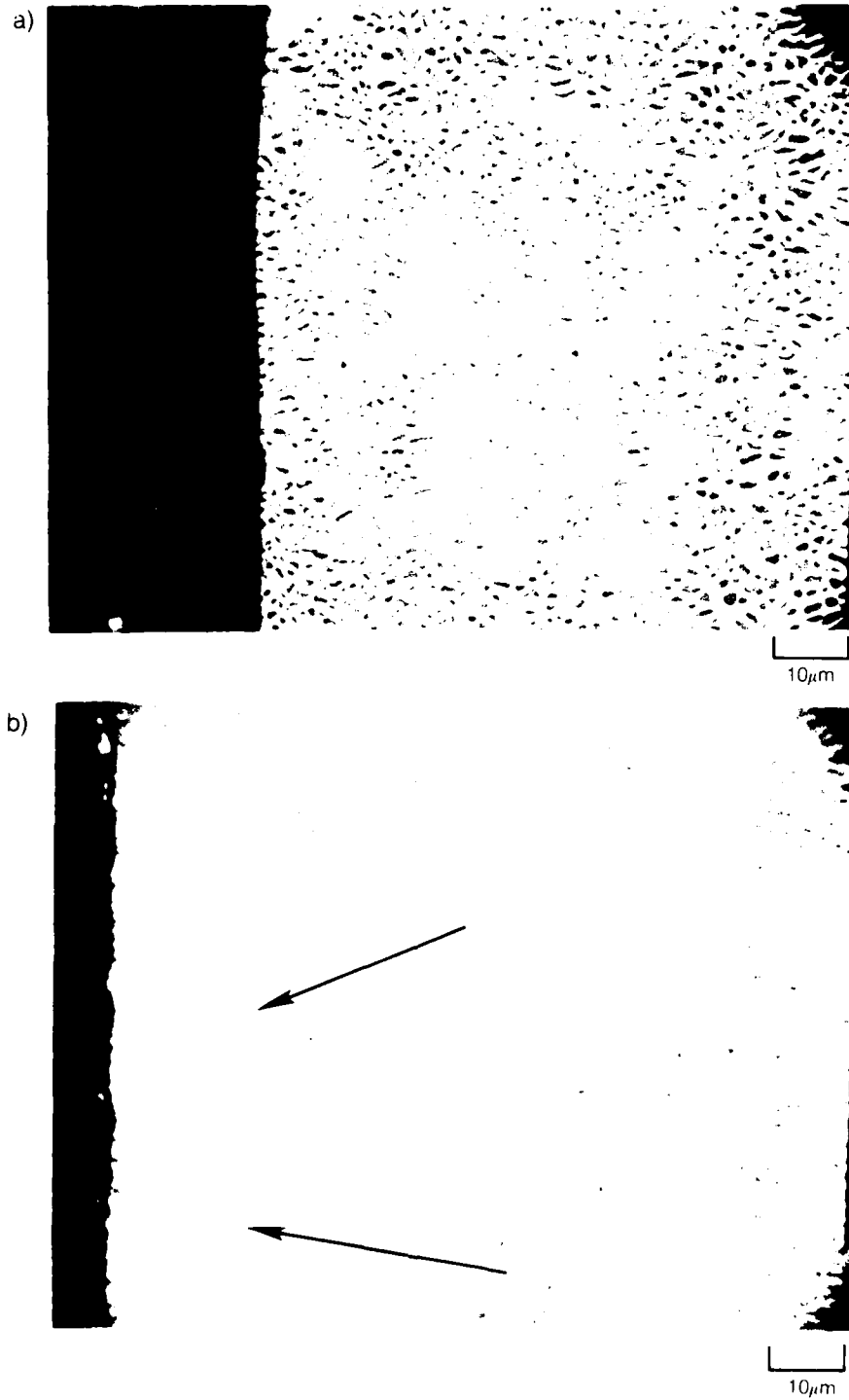
Figure 10. Backscattered Electron Image of Laser-Processed Zone
a) NiCrAl
b) NiCrAlHf Showing Hafnium Rich Particles (Arrows)

500 μm

Figure 11. Backscattered Electron Micrograph of Surface of Laser-Processed NiCrAl
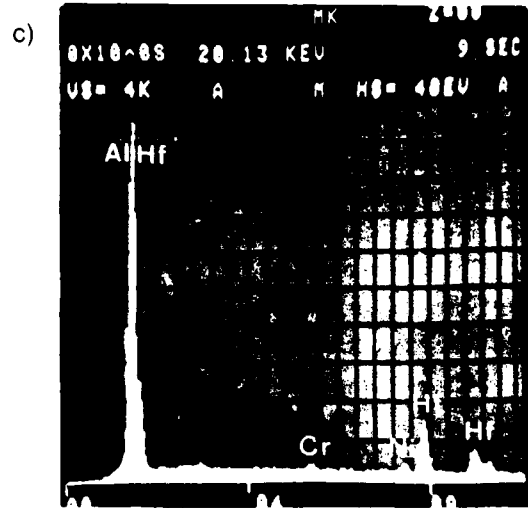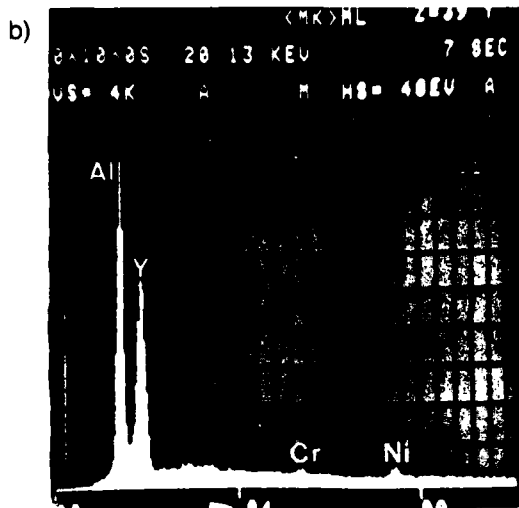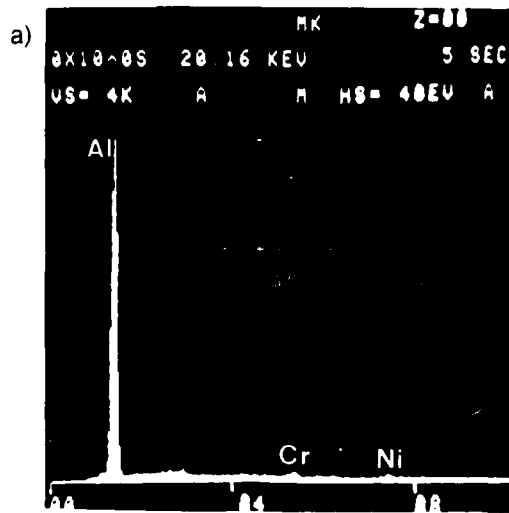
Figure 12. X-ray Spectrum of Slag Particles on Laser-Processed Surfaces of
a) NiCrAl
b) NiCrAlY
c) NiCrAlHf
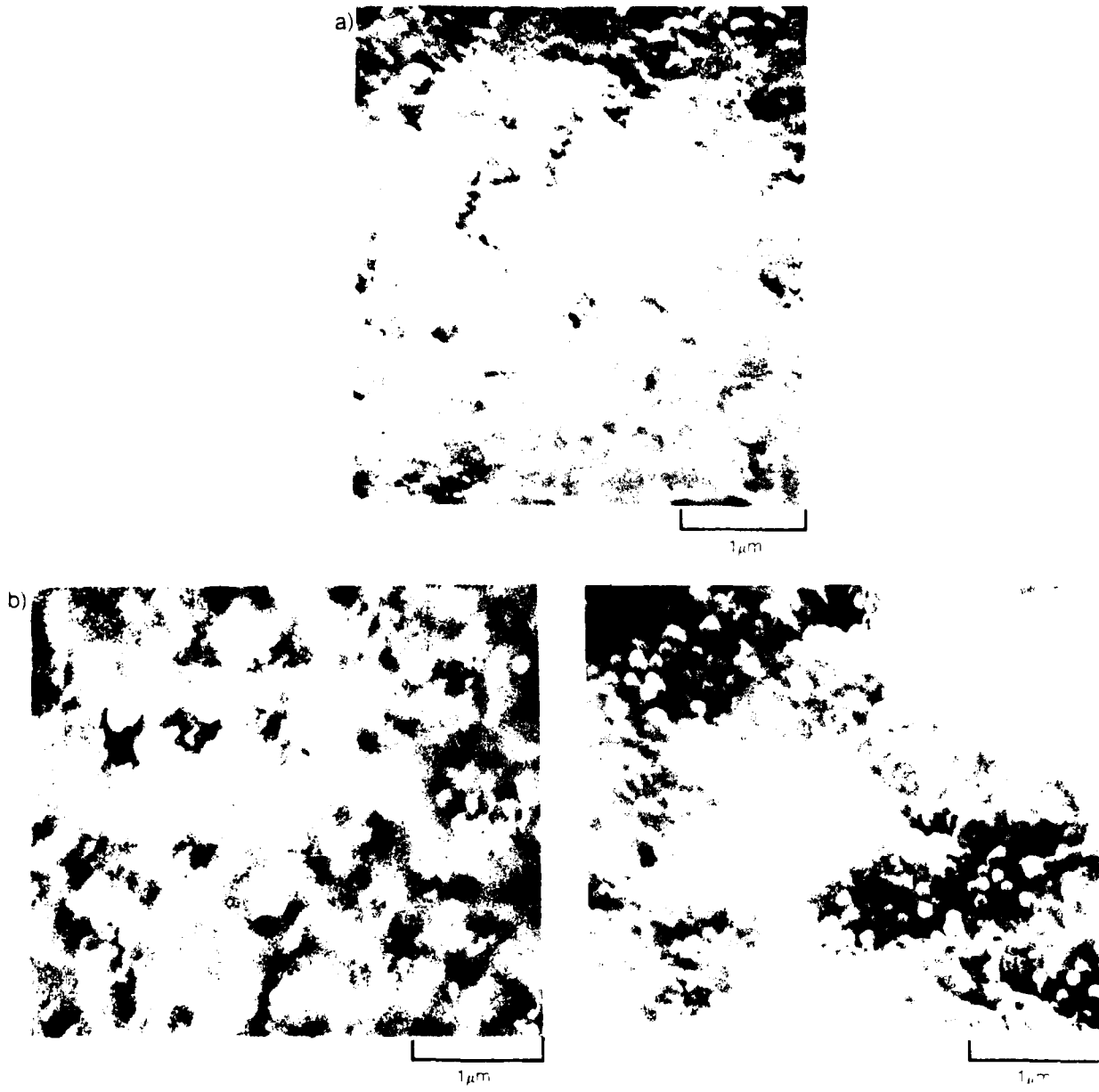
Figure 13. Electron Micrograph of the Laser-Processed Surfaces of
a) NiCrAl
b) NiCrAlY
c) NiCrAlHf
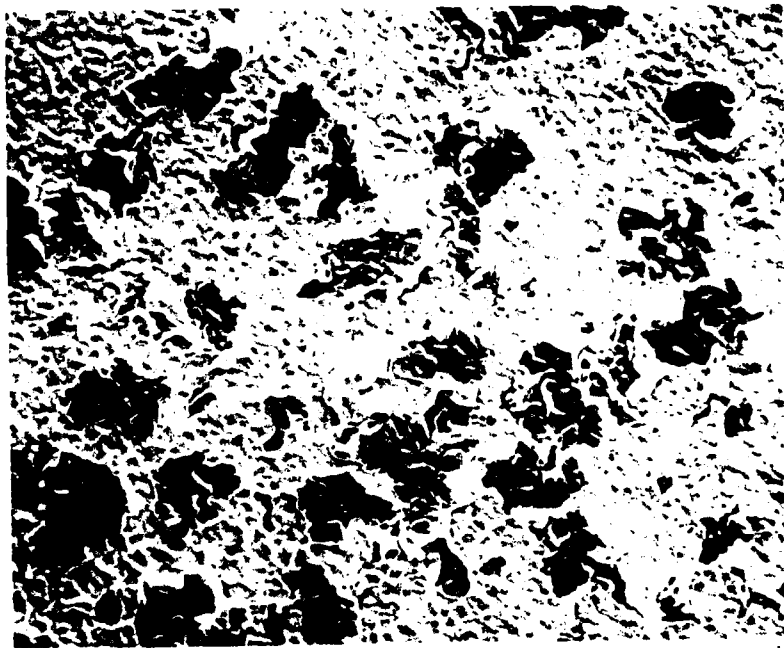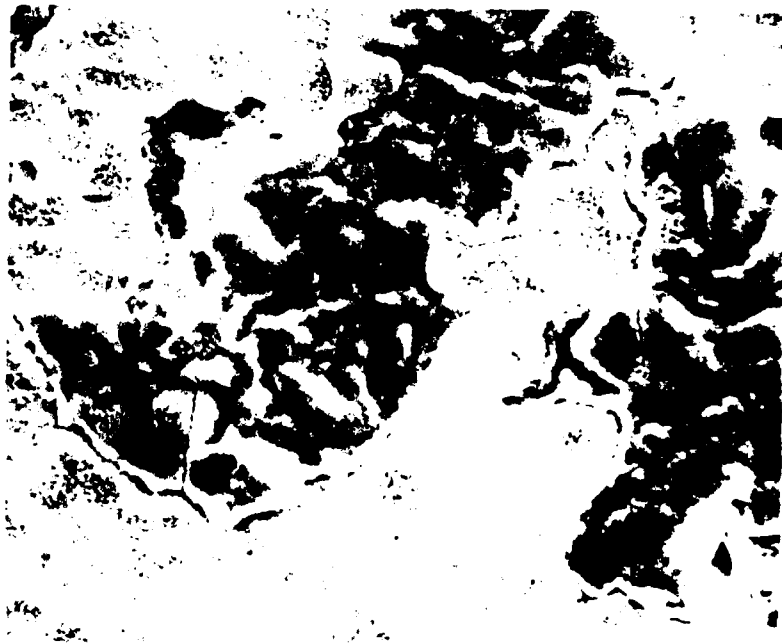
100μm

Figure 14. NiCrAl After 100 hours of Isothermal T~~ ,'ng at 1050°C
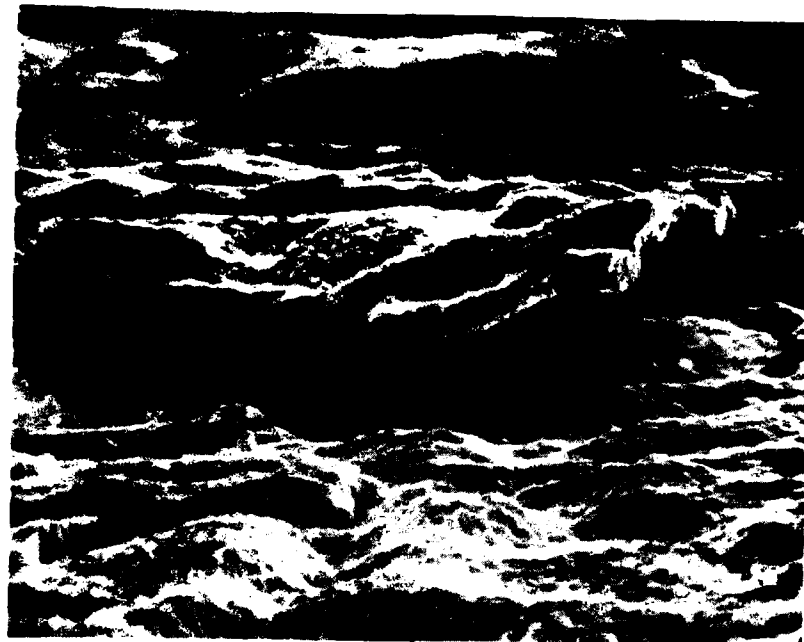
Figure 15. Microstructure of Oxide Scales Over NiCrAl. 100 hours Isothermal Test
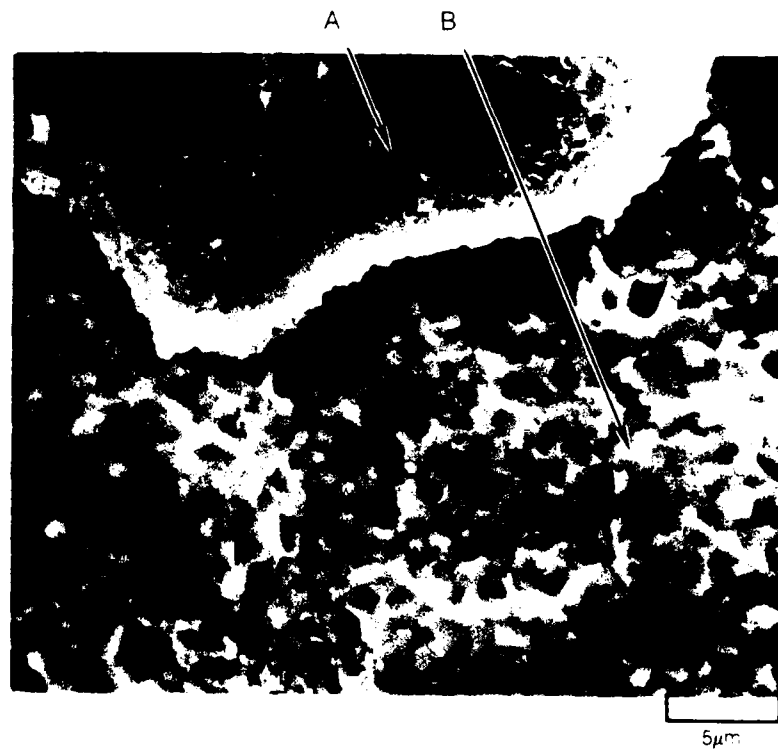
Figure 16. Locally Retained Oxide (A) and Adjacent Substrate Metal (B).
Porosity in External Oxide Layer.
Facetting in Metal Surface.
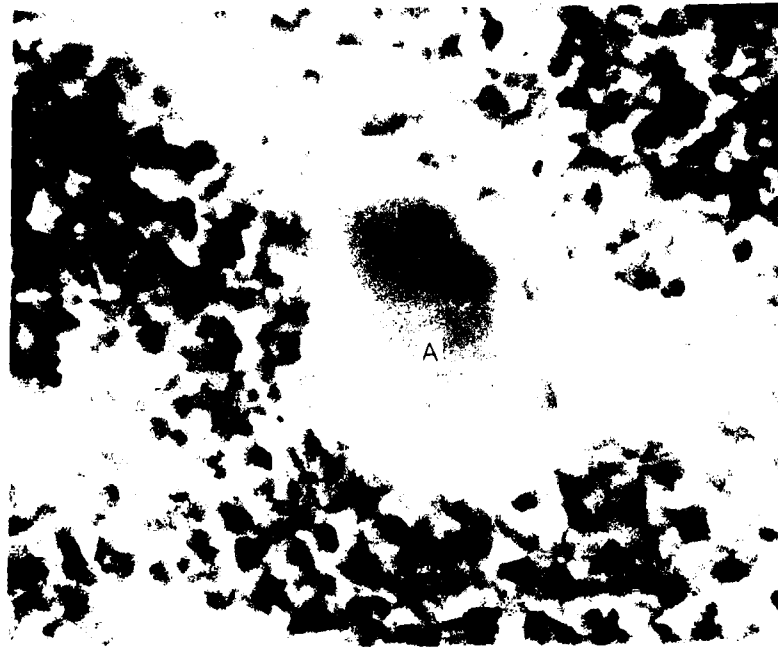
Figure 17. Local Kirkendall Pore (A) On Surface of NiCr Al Specimen After 100 hours of Isothermal Testing. Note General Facetting of the Neighboring Metal Surface

1μm
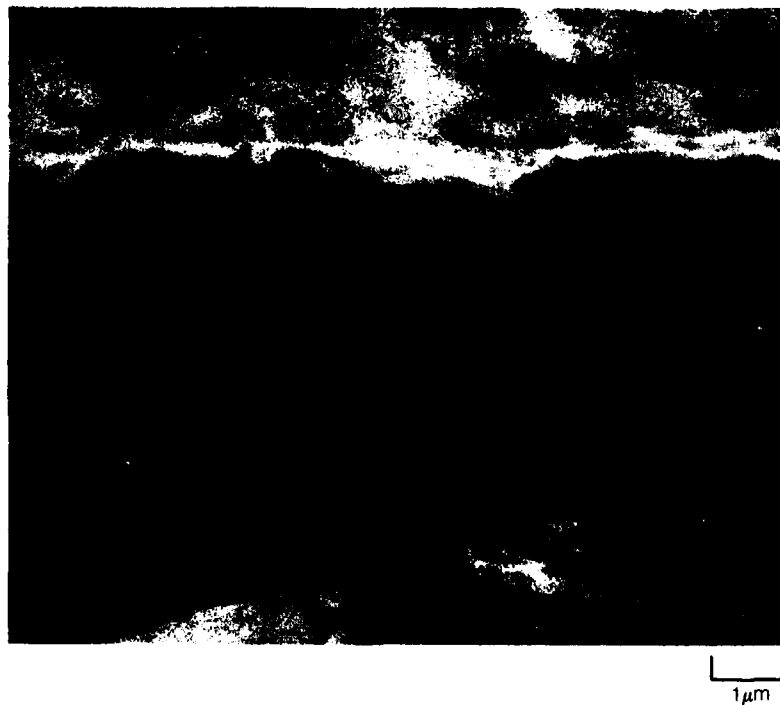
Figure 18. Typical Edge View of the Fractured Alumina Scale on Laser-Processed Surface NiCrAl After 100 hours of Isothermal Testing at 1050°C
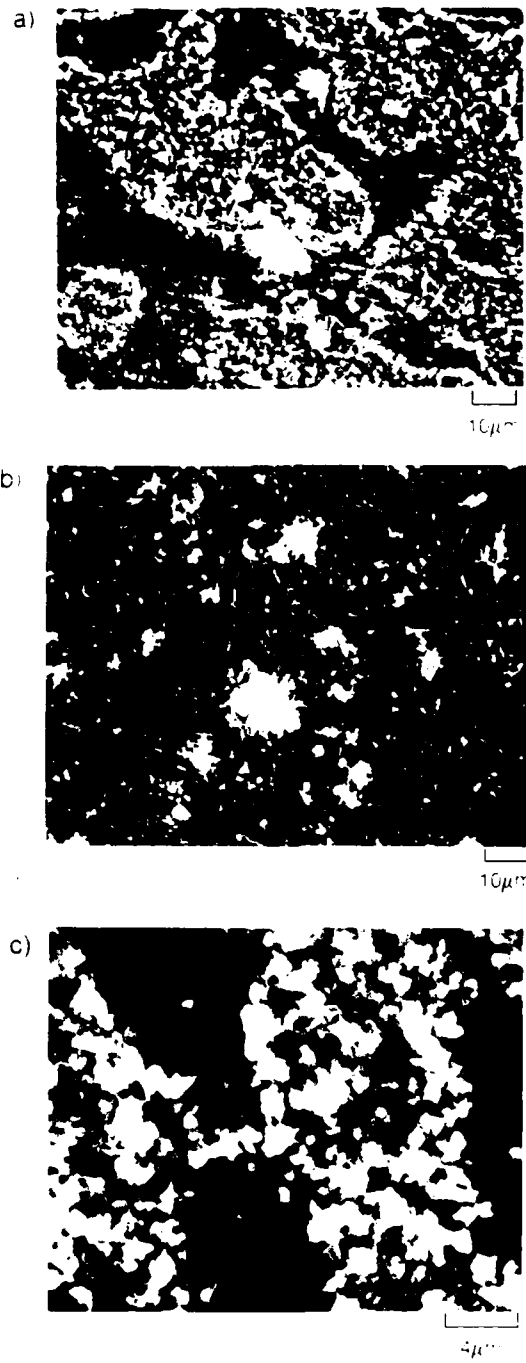
Figure 19. NiCrAlHf After 100 hours Isothermal Oxidation at 1050 °C
a) Secondary Electron Micrograph
b) Back-scattered Electron Micrograph
c) Nodular Oxide Growths Over β-NiAl
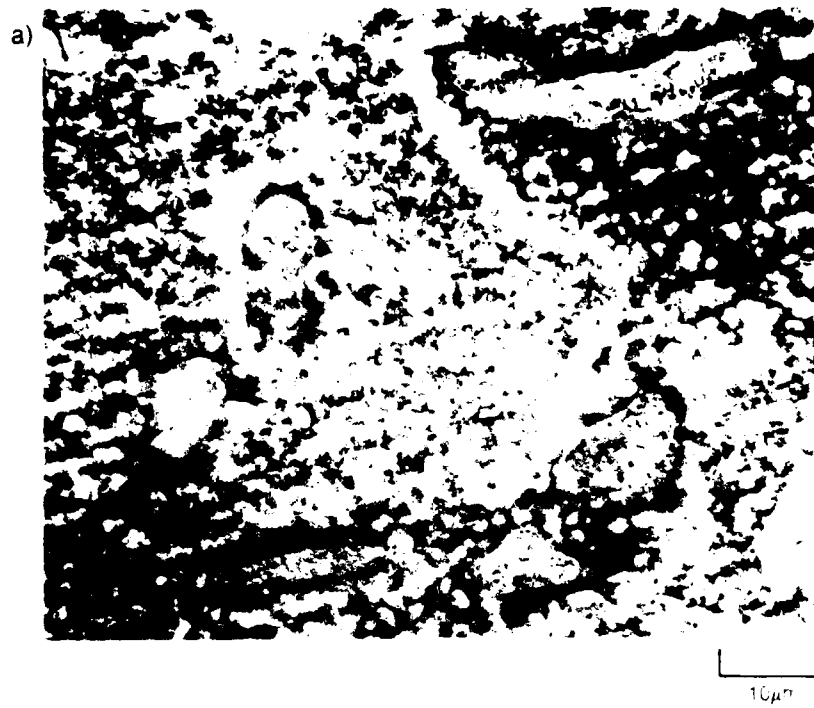
Figure 20. NiCrAlHf After 100 hours Cyclic Oxidation at 1050°C
a) Secondary Electron Micrograph
b) Back-scattered Electron Micrograph

Figure 21. Typical Area of Laser-Processed NiCrAlHf Isothermally Tested for
100 hours in Regions Away From Slag Lines
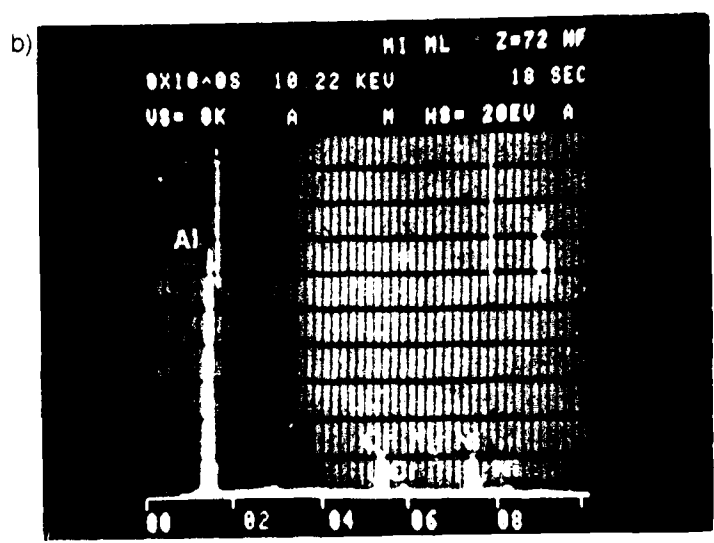
Figure 22. Laser-Processed NiCrAlHf Surfaces After Isothermal Testing at 1050°C for 100 hours. 1) Adherent Scale, 2) Local Scale Exfoliation, 3) Slag Line
a) Scanning Electron Micrograph
b) EDAX of Adherent Retained Oxide
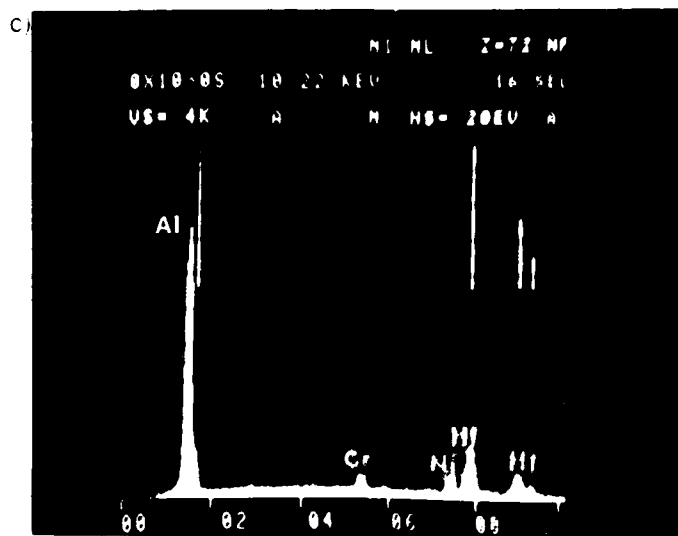
Figure 22. Laser Processed NiCrAlHf Surfaces After Isothermal Testing at 1050°C for 100 hours.

    a) Scanning Electron Micrograph. (500 ×)
        1. Adherent Scale
        2. Local Scale Exfoliation
        3. Slag Line
    b) Energy Dispersive Analysis of Adherent Retained Oxide.
    c) Energy Dispersive Analysis of Retained Slag.

a)

b)
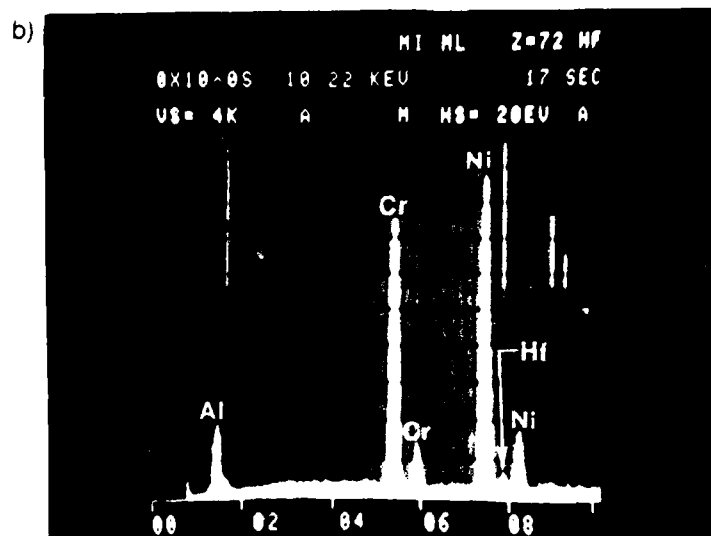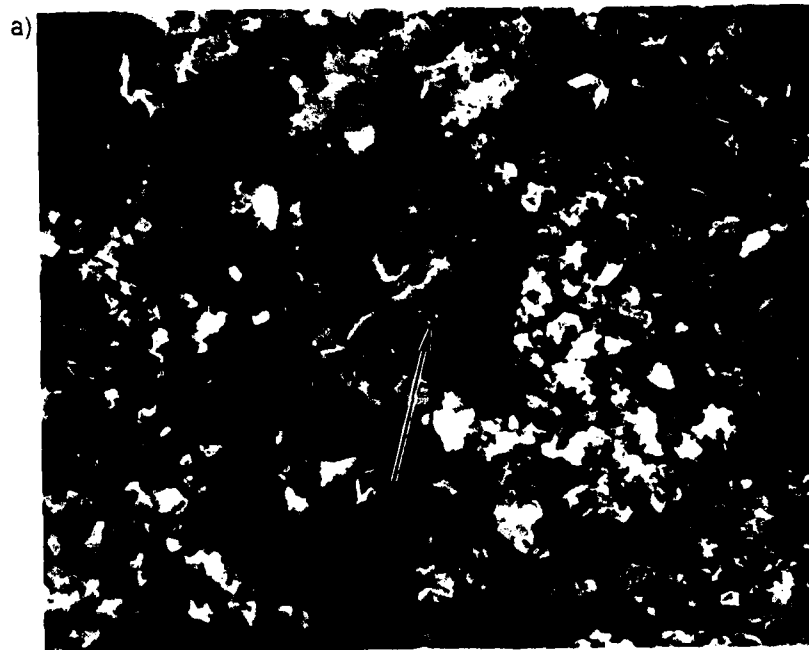
Figure 23. Formation of Less Protective Nickel and Chromium-Rich Scales
Produced Subsequent to Isothermal Scale Exfoliation, cf. Fig. 22 (Area 2).
a) Scanning Electron Micrograph.
b) Energy Dispersive Analysis of Reformed Scale.
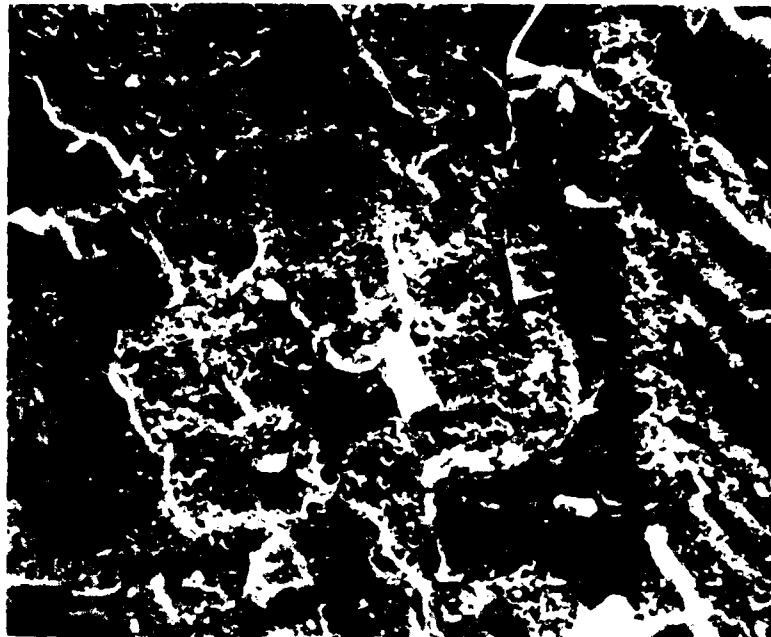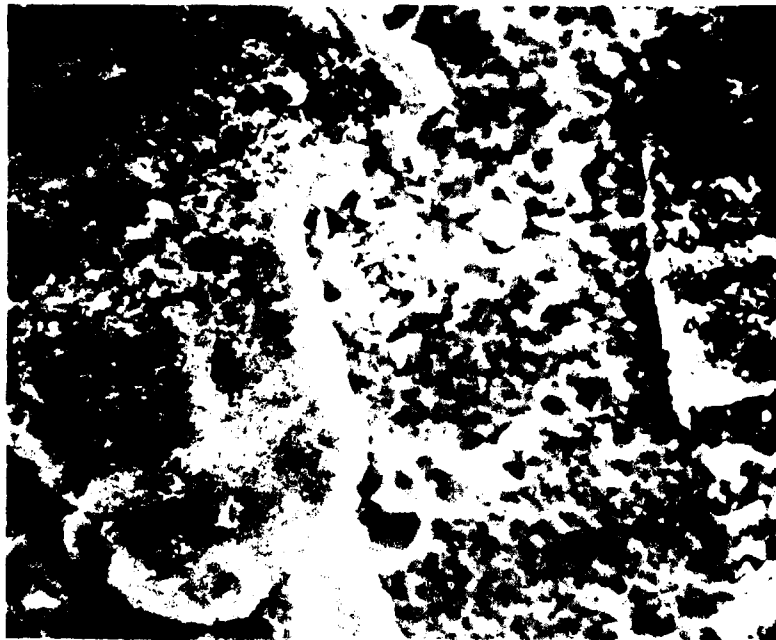
Figure 24. Laser-Processed NiCrAlHf Specimen After 100 hours at 1050°C

a)

100μm

b)

20μm
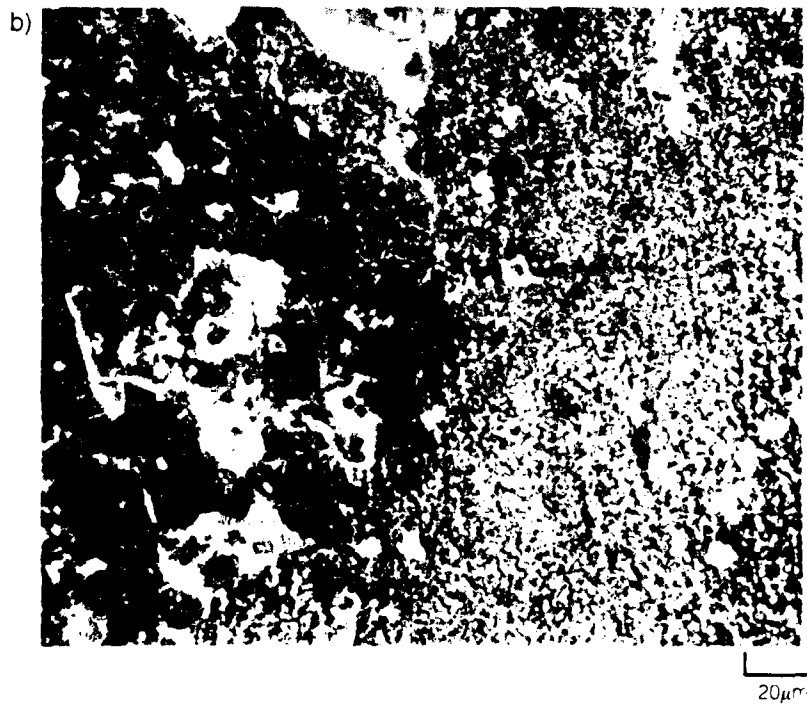
Figure 25. Laser-Processed Then Abraded NiCrAlHf After 100 hours of
Isothermal Testing at 1050°C.
a) Overall Uniform Scale Morphology.
b) Local Scale Exfoliation.

83-10-11 25

20μm
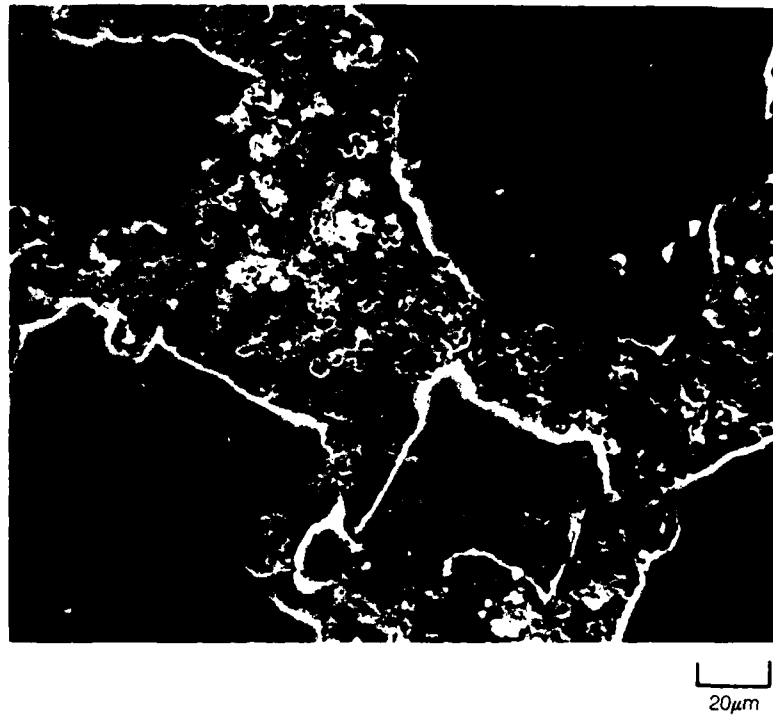
Figure 26. Laser-Processed and Abraded NiCrAlHf Specimen Subsequently Oxidized at 1050°C for 100 hours.
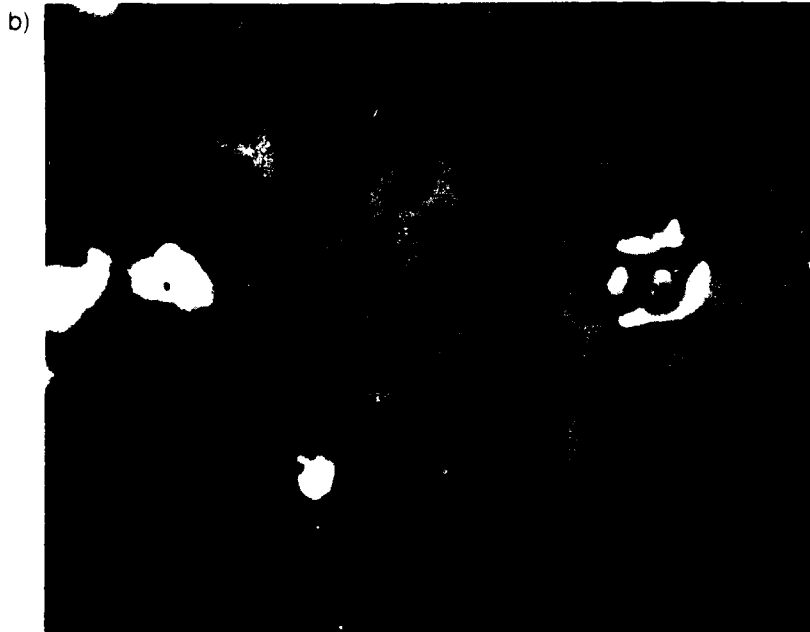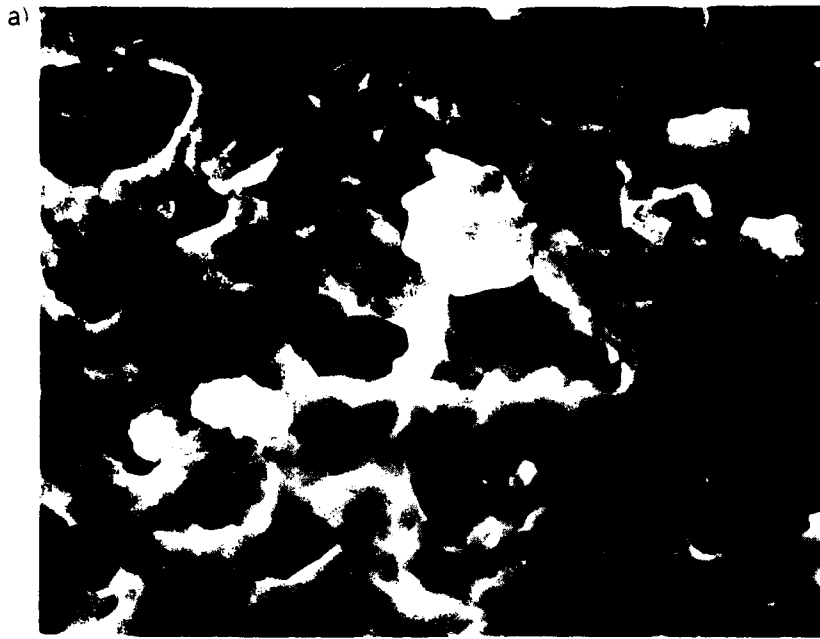
Figure 27. Retained Oxide Pegs. Surface of Cyclically Tested Laser-Processed NiCrAlHf Where Scale Has Exfoliated.
a) Scanning Electron Micrograph.
b) Back-Scattered Electron Micrograph. (Slightly Shifted)

20μm
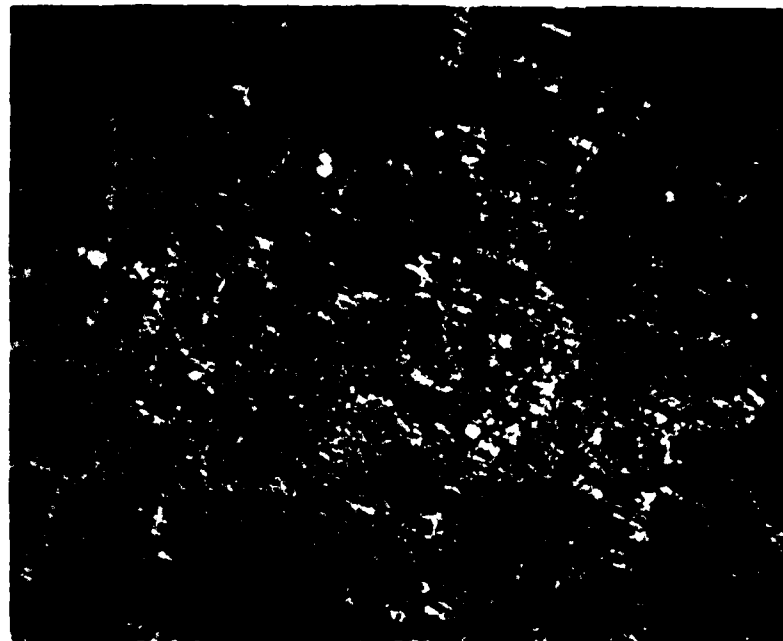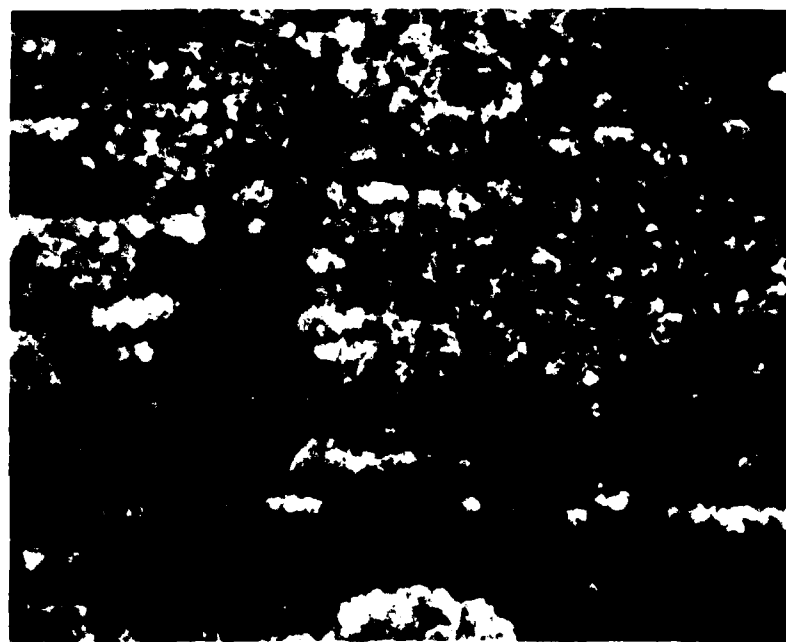
5μm

Figure 28. NiCrAlY After 100 hours of Isothermal Testing at 1050°C

83–10–11–22

a)

5μm

b)

5μm
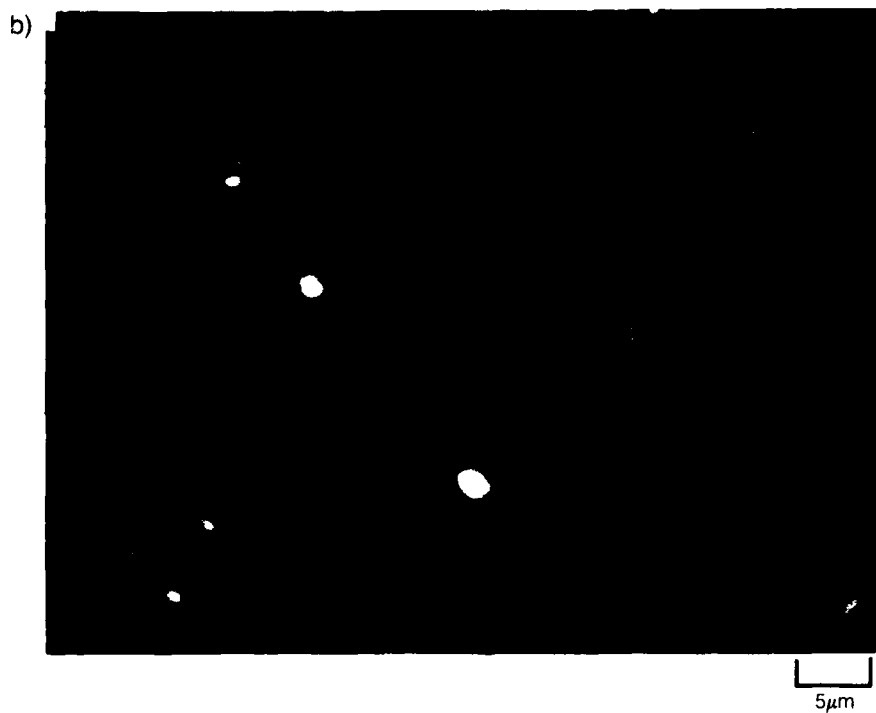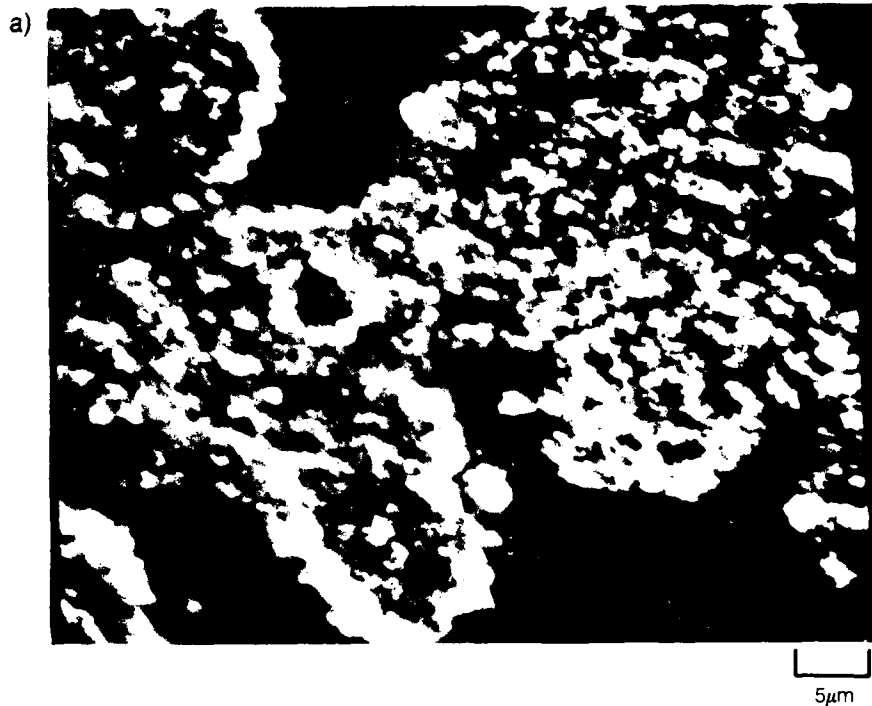
Figure 29. Localized Yttrium Distribution in Oxide Scale Formed on NiCrAl After 100 hours Isothermal Testing at 1050°C.
a) Secondary Electron Micrograph
b) Back Scattered Electron Micrograph
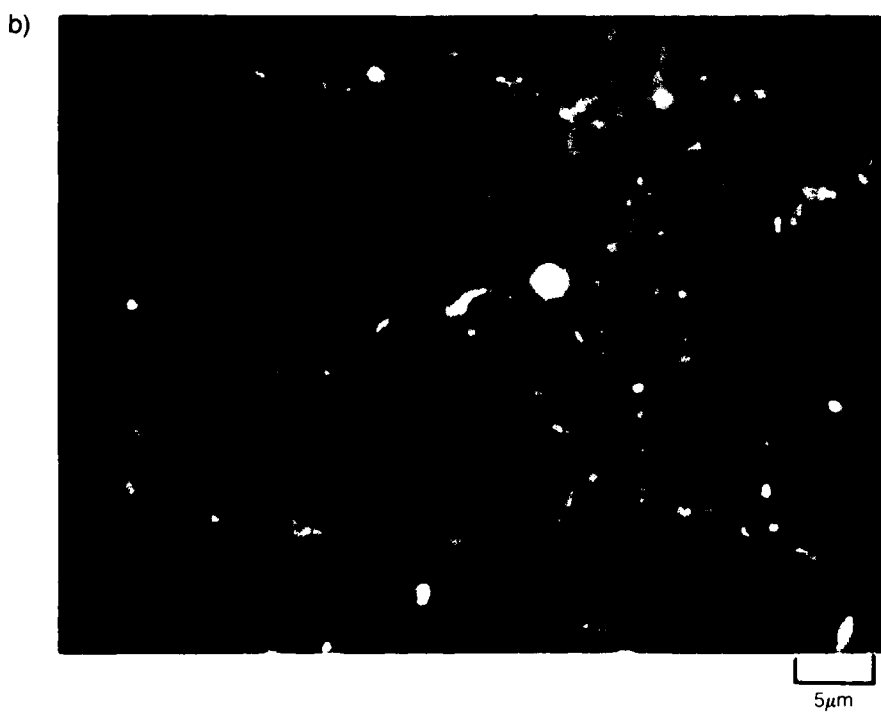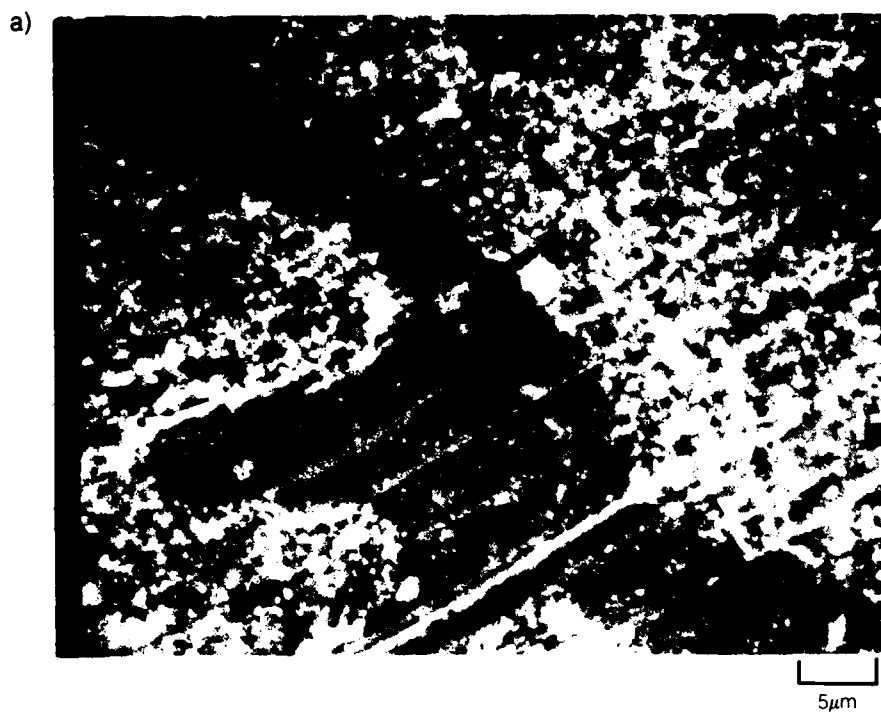
Figure 30. Yttrium Distribution in Oxide Scales Formed on NiCrAlY After 100 hours of Thermal Cycling at 1050°C
a) Scanning Electron Micrograph
b) Back Scattered Electron Micrograph

20μ

5μm
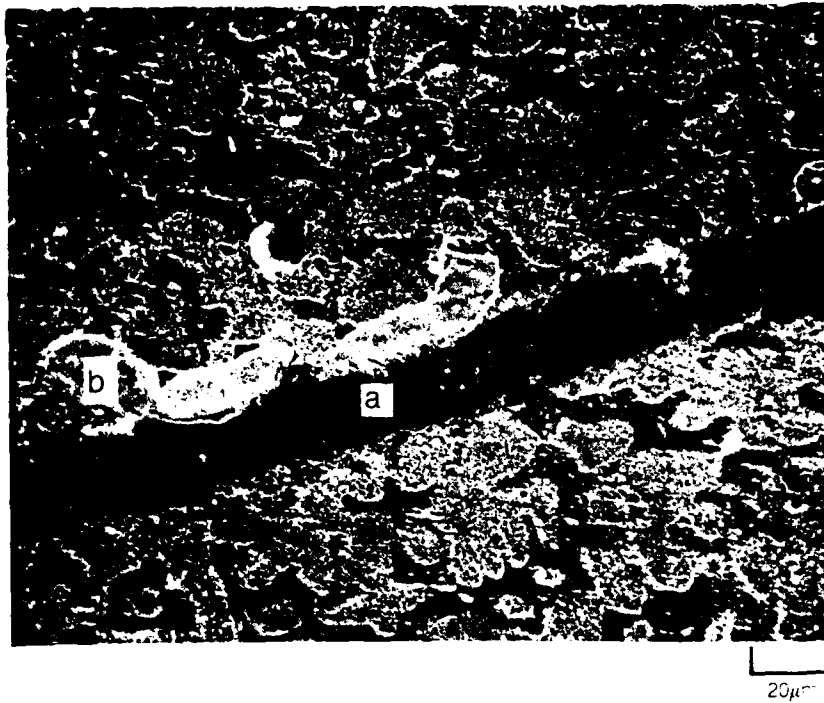
Figure 31. Abrasion Track on Oxide Scale on Isothermally Tested NiCrAlY Specimen
a) Abrasion Path
b) Local Scale Exfoliation
c) Cracks in Alumina Scale Within Wear Path
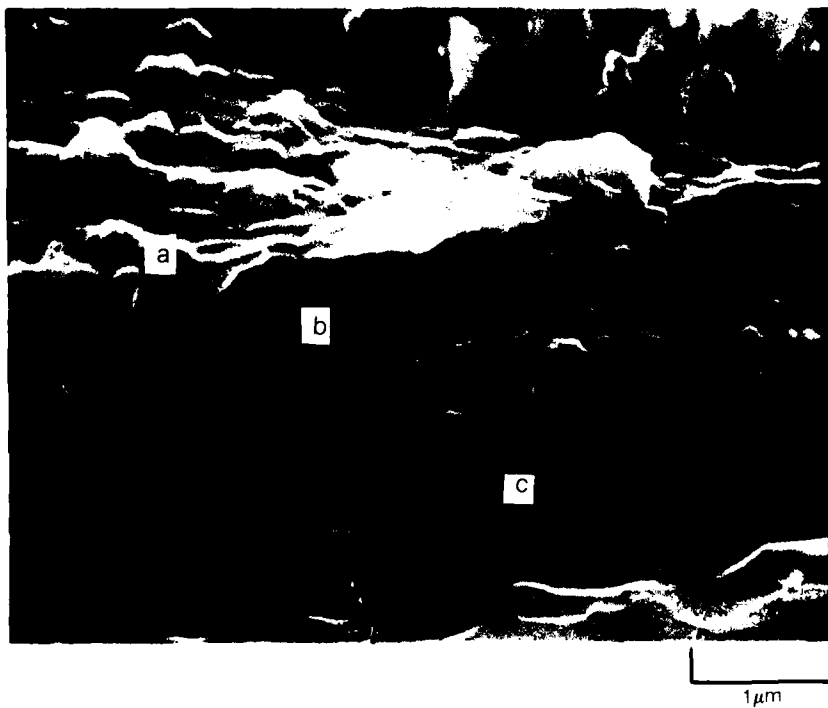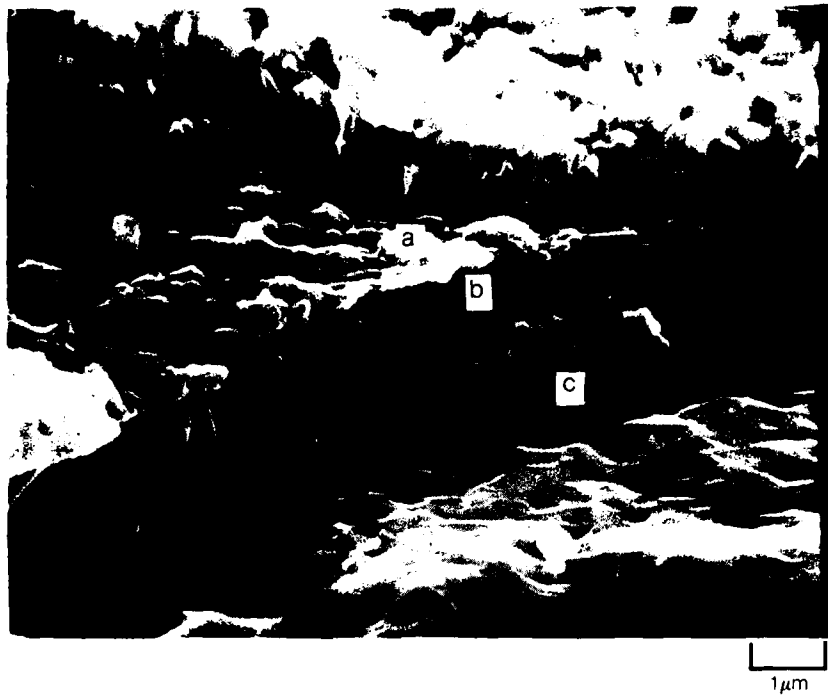
Figure 32. Oxide Scale Over Nickel Solid Solution (Isothermal Test)
a) 0.1 micron Outermost Oxide Layer
b) 0.75 micron Fine Grained (Porous ?) Layer
c) 1.5 micron Innermost Columnar Oxide Layer

20μm
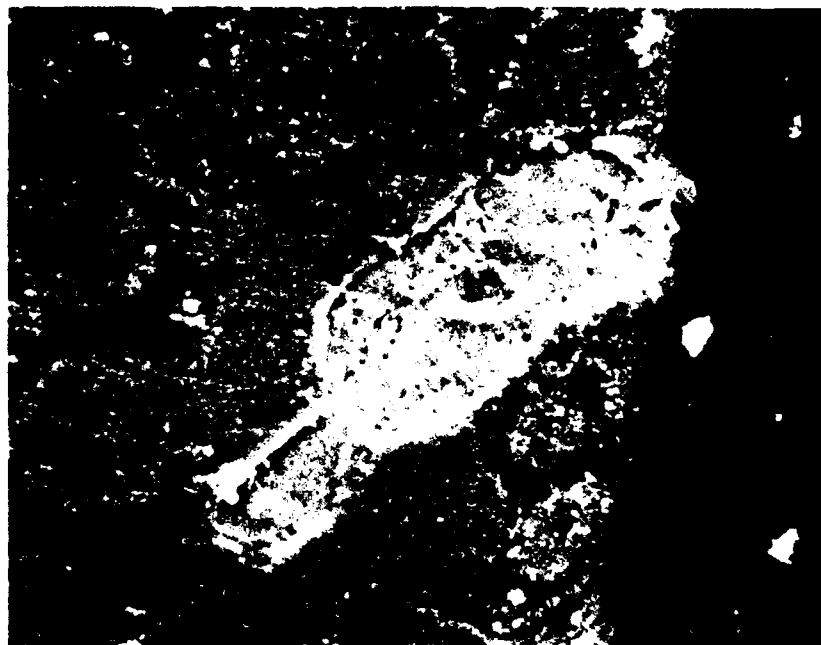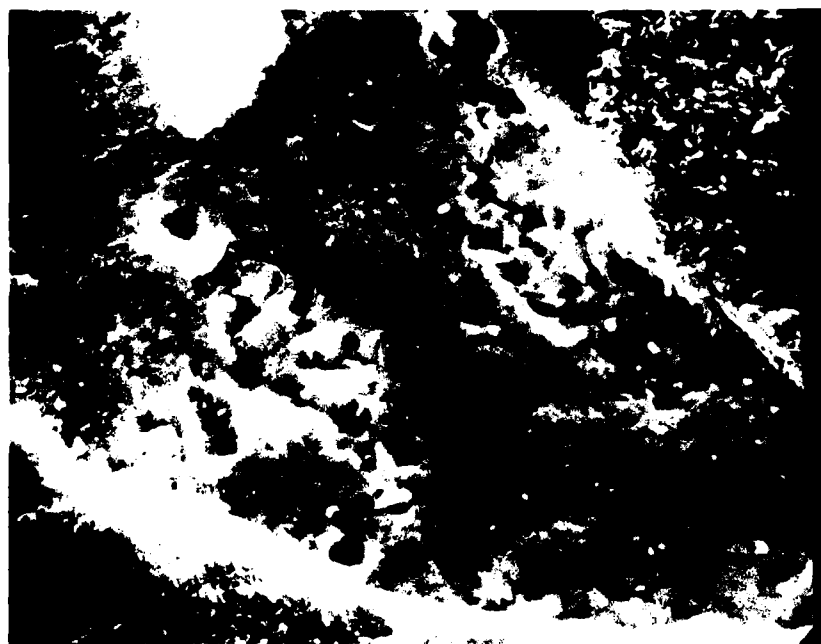
5μm

Figure 33. Microporosity in NiCrAlY at Base of Oxide Scale. Isothermally Tested at 1050°C for 100 hours. Diamond Scribed Prior to Examination.

83-10-11-17

Figure 34. Oxide Scale Over β-NiAl (Isothermal Test)
a) 2.8 micron Nodular (Porous) Layer
b) 1.5 micron Innermost Columnar Oxide Layer
c) Macroscopic Pore in Substrate
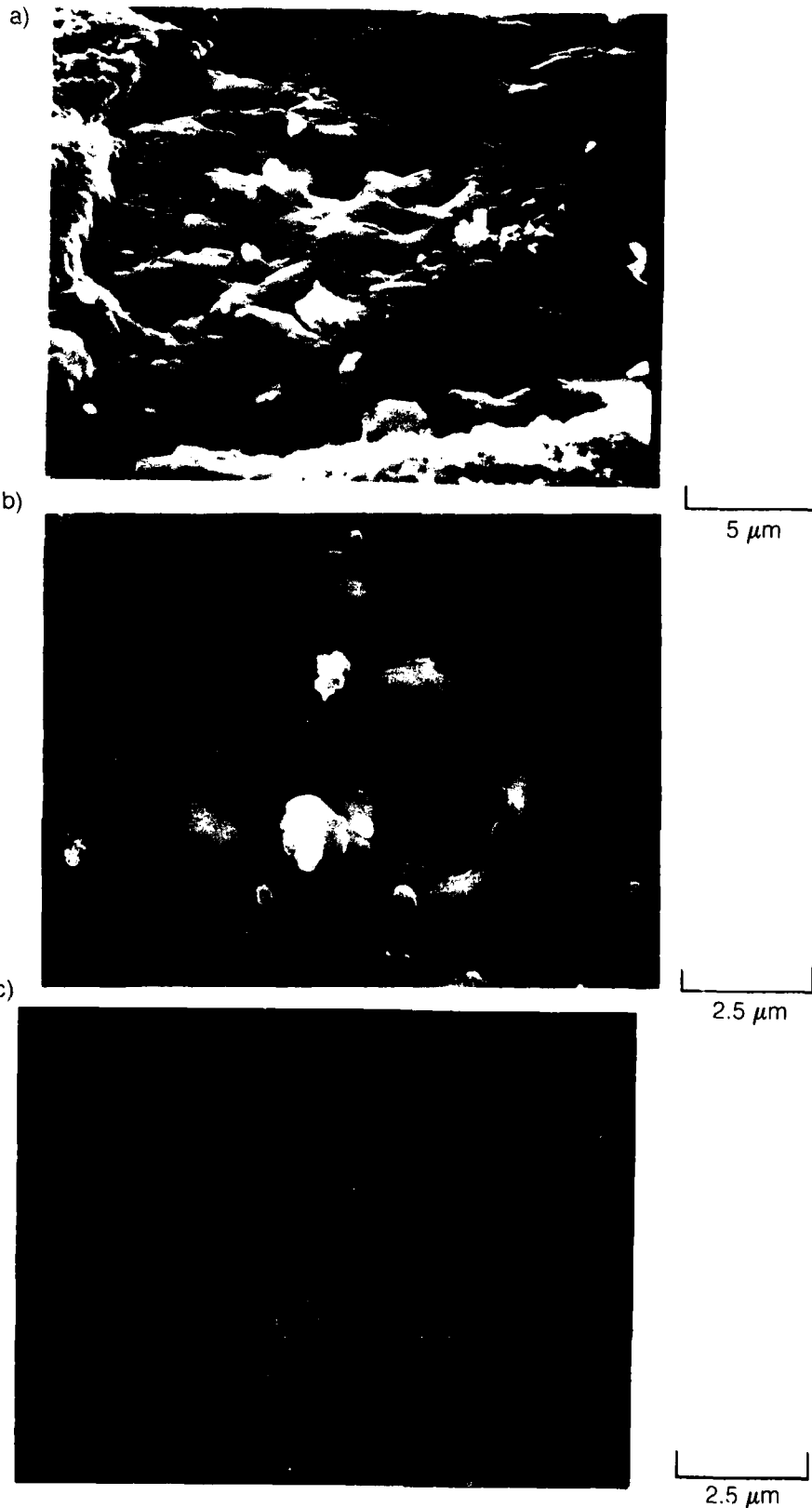
Figure 35. Micropeg at Base of Abraded Oxide Scale. NiCrAlY Isothermally Oxidized at 1050°C for 100 hours
a) and b) Secondary Electron Micrographs
c) X-ray Map: Yttrium

20μ
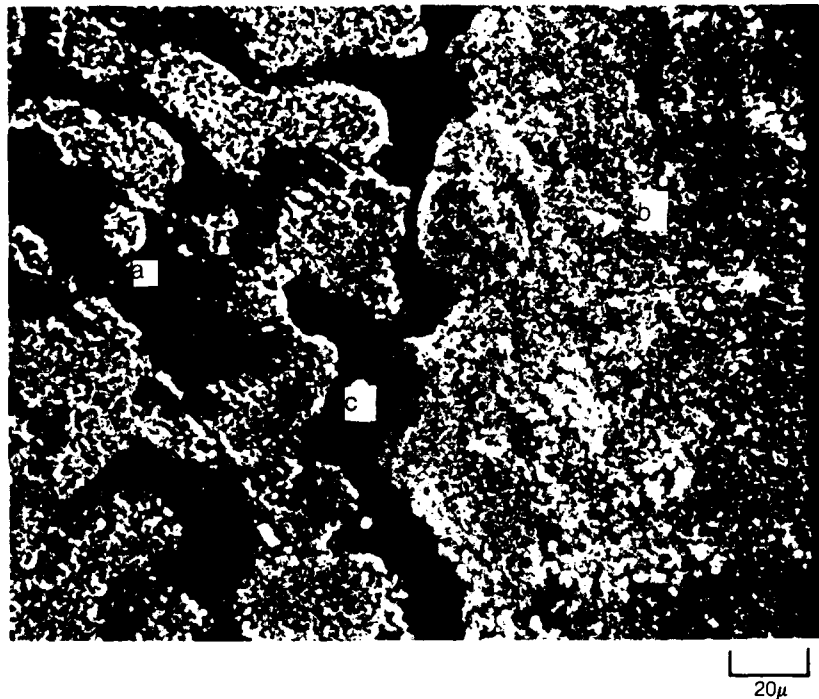
Figure 36. Interface Between Laser-Processed Surface and Annealed Surface.
NiCrAlY Isothermally Tested at 1050°C for 100 hours
a) As-annealed Surface
b) Laser Heated Surface
c) Aluminum-yttrium Enriched Slag Bead at Interface (Produced During
Laser Processing and Retained During This Test Condition)
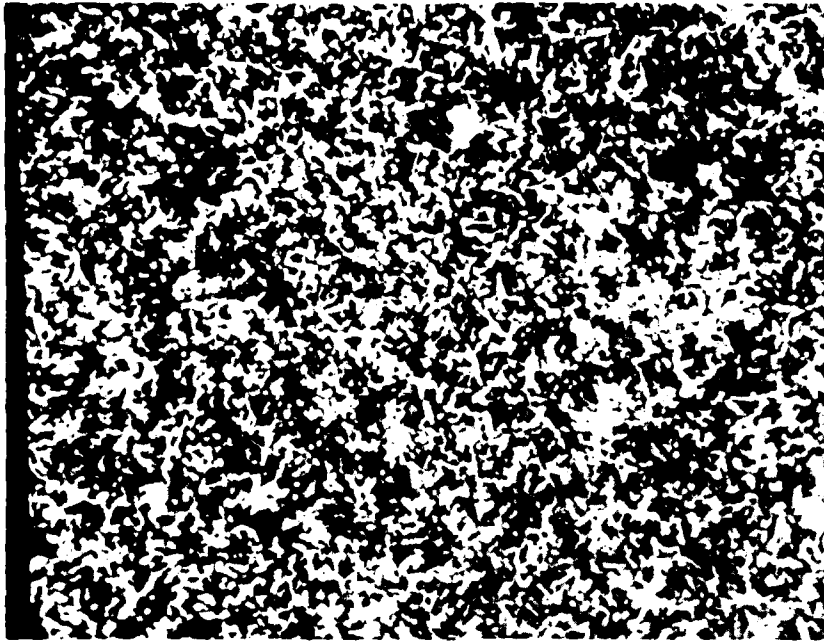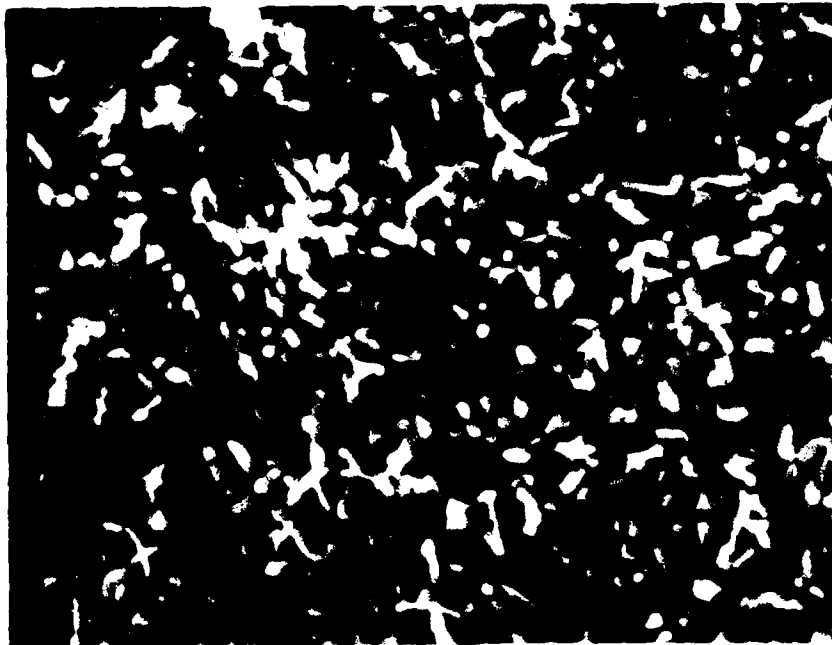
Figure 37. Oxide Scale Produced on Laser-Processed Surfaces of NiCrAlY After 100 hours of Isothermal Testing at 1050°C
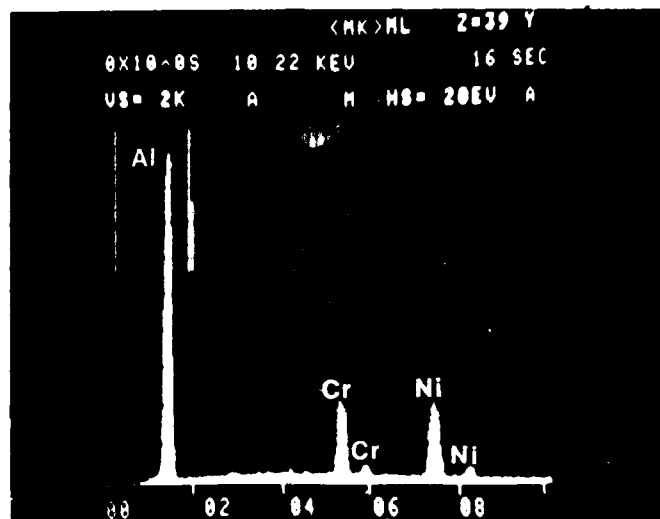
Figure 38. Absence of Yttrium in Oxide Scales. Energy Dispersive X-ray Analysis of the Entire Area Shown in Fig. 37A. (Presence of Cr and Ni Result from the Electron Beam Probing Through the Oxide Layer to the Underlying Metal)

1μm

Figure 39. Laser-Processed NiCrAlY Surface After 100 hours at 1050°C
Mechanically Scribed Surface. Partially Detached Oxide Scale in
Cross Section.
a) Alumina Whiskers
b) Substrate Metal
c) Absence of any Significant Oxide Pegs Protruding from Base of
Scale into Substrate
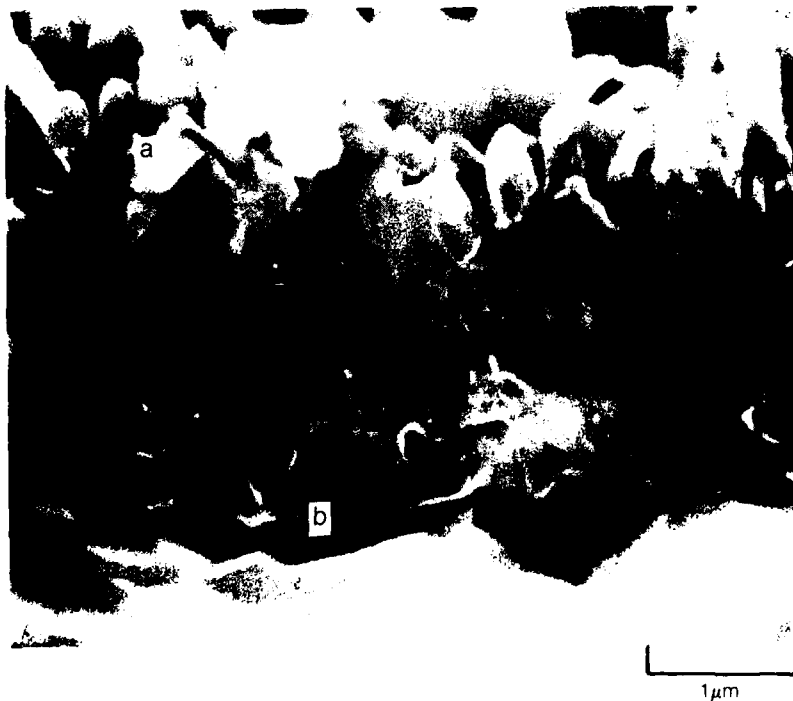
Figure 40. Oxide Scale Structure. Laser-Processed NiCrAlY Isothermally Tested at 1050°C for 100 hours
a) 2.5 micron Porous Oxide Layer
b) 0.5 micron Dense Scale

20μm
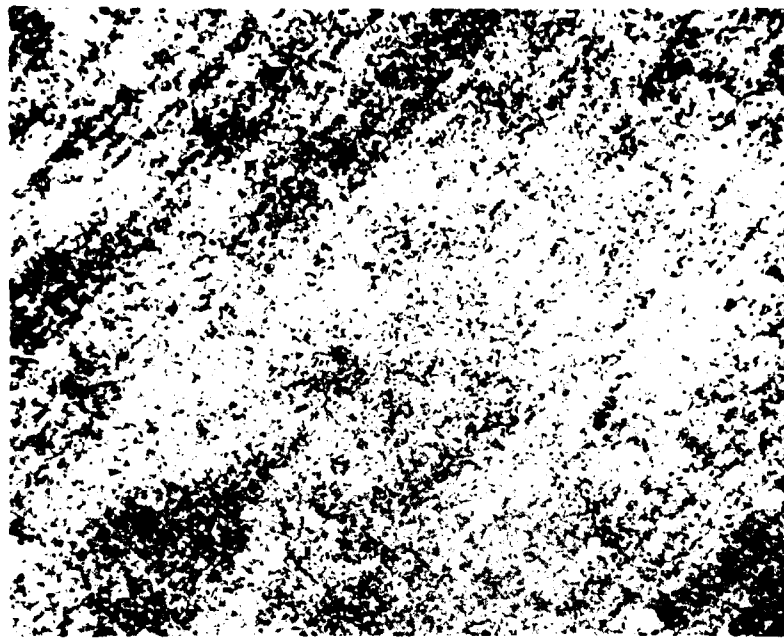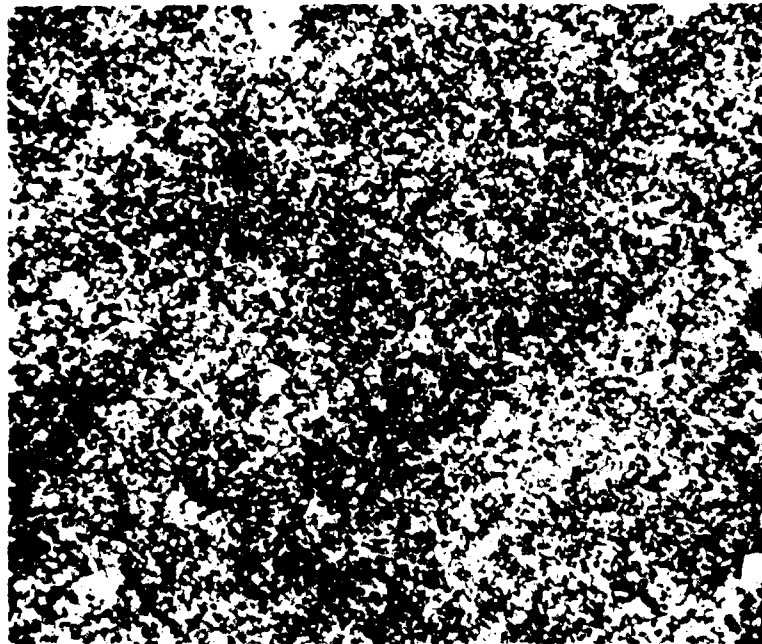
10μm

Figure 41. Laser-Processed NiCrAlY Surface Subsequently Abraded with 600 Grit SiC to Remove
Initial Oxide Scale Prior to 100 hour Isothermal Test at 1050°C.
(Post-test Micrograph)

83—10—11—9
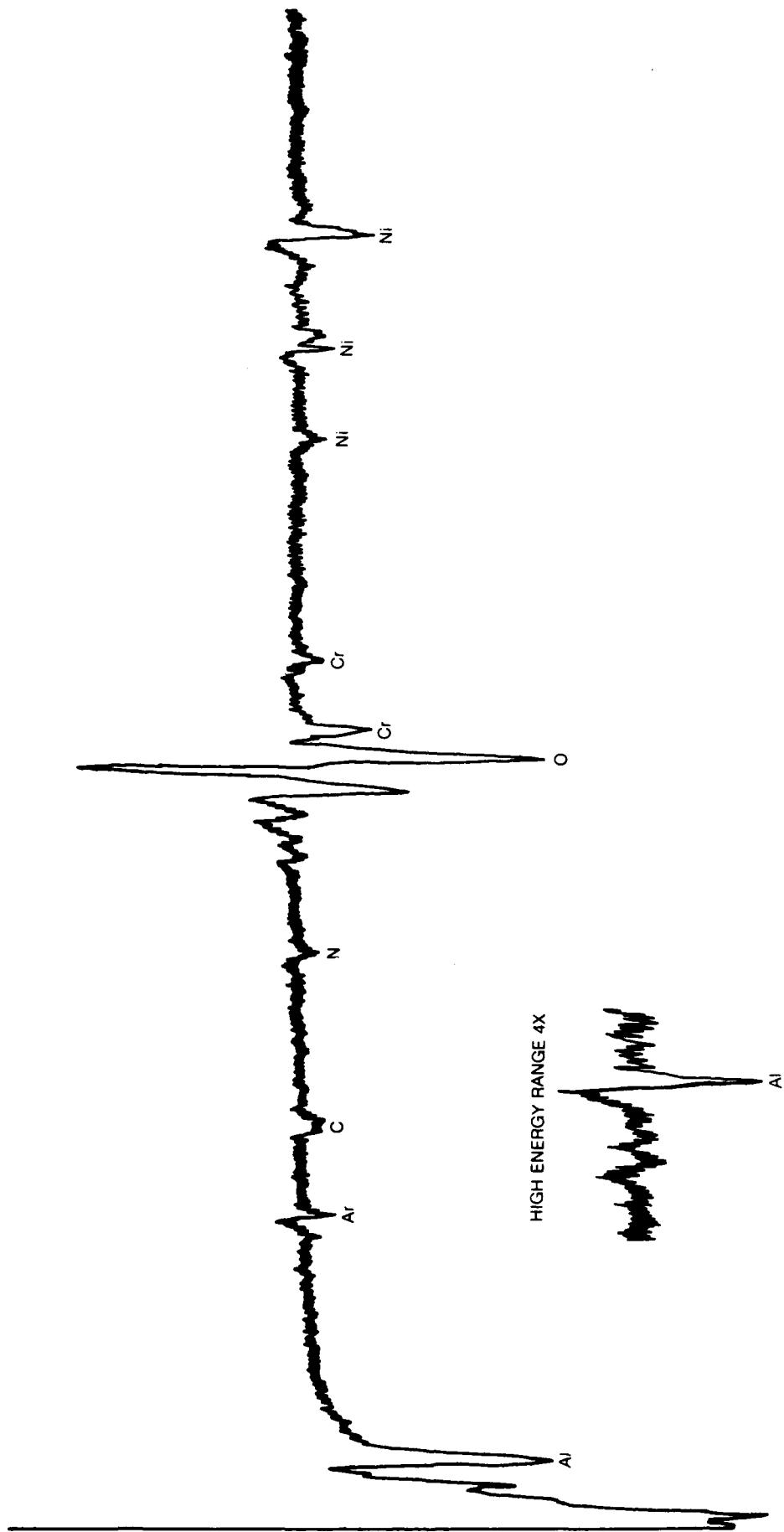
**Figure 42. Auger Spectrum for Polished and Sputtered NiCrAl Surface**

HIGH ENERGY RANGE 4X

83—5—62—15
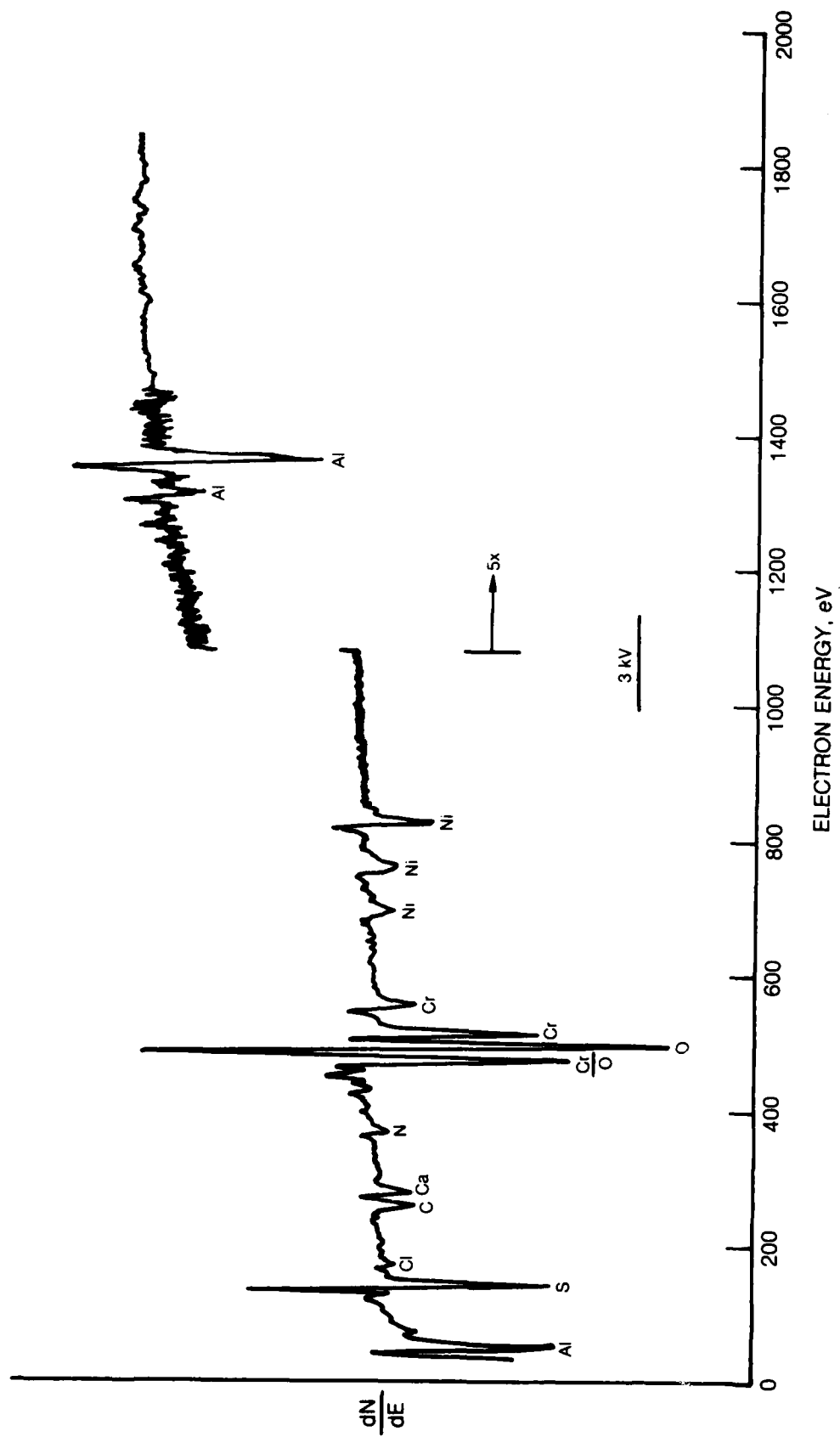
Figure 43. Auger Spectrum of Polished and Sputtered NiCrAl Heated to 700°C

83—1—100—7
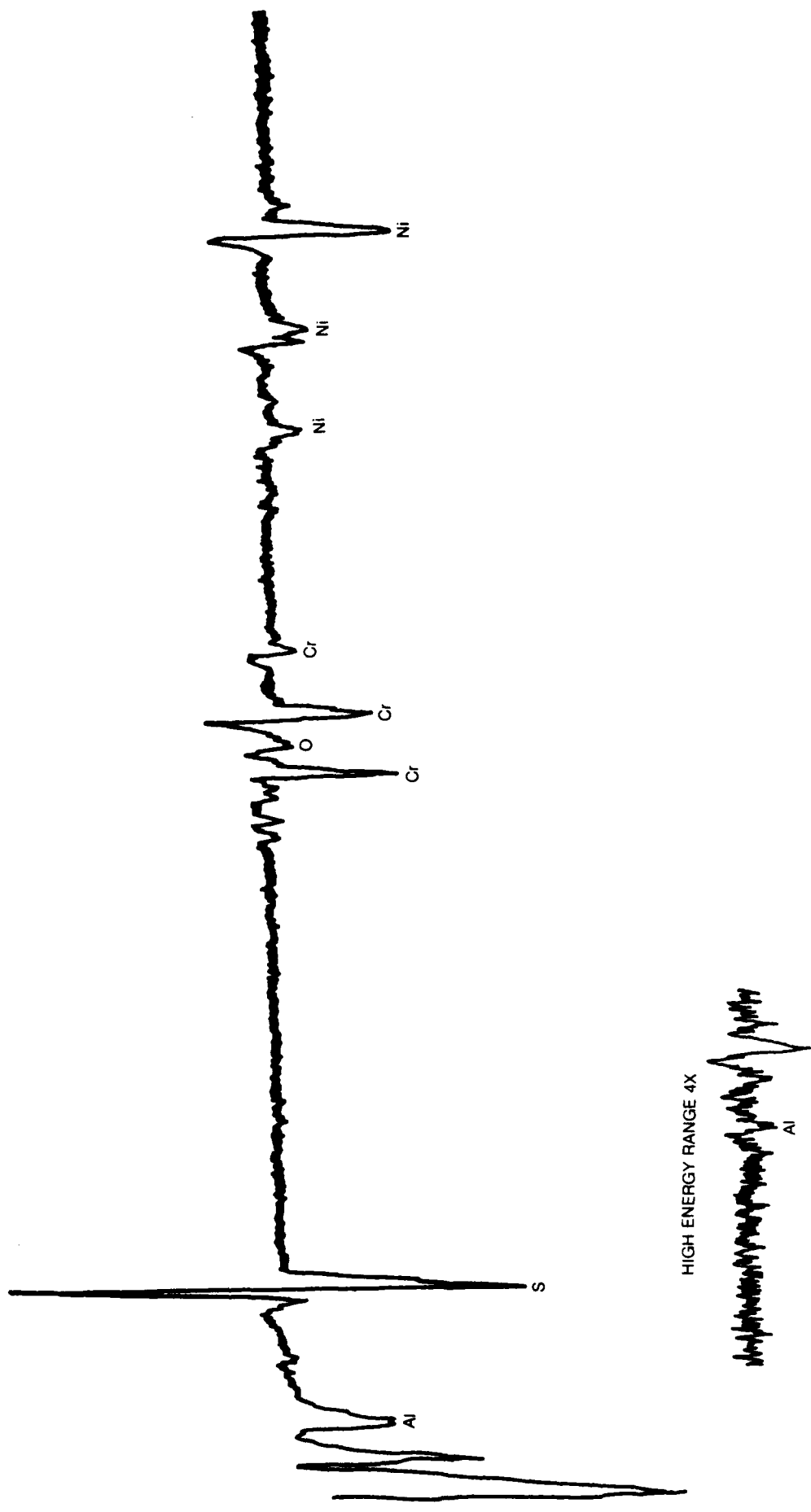
Figure 44. Auger Spectrum for NiCrAl at 1000°C

83-5-62-16

Figure 45. Auger Spectum for Laser-Processed NiCrAl

83—1—100—6

ELECTRON ENERGY, eV

$\dfrac{dN}{dE}$

5x
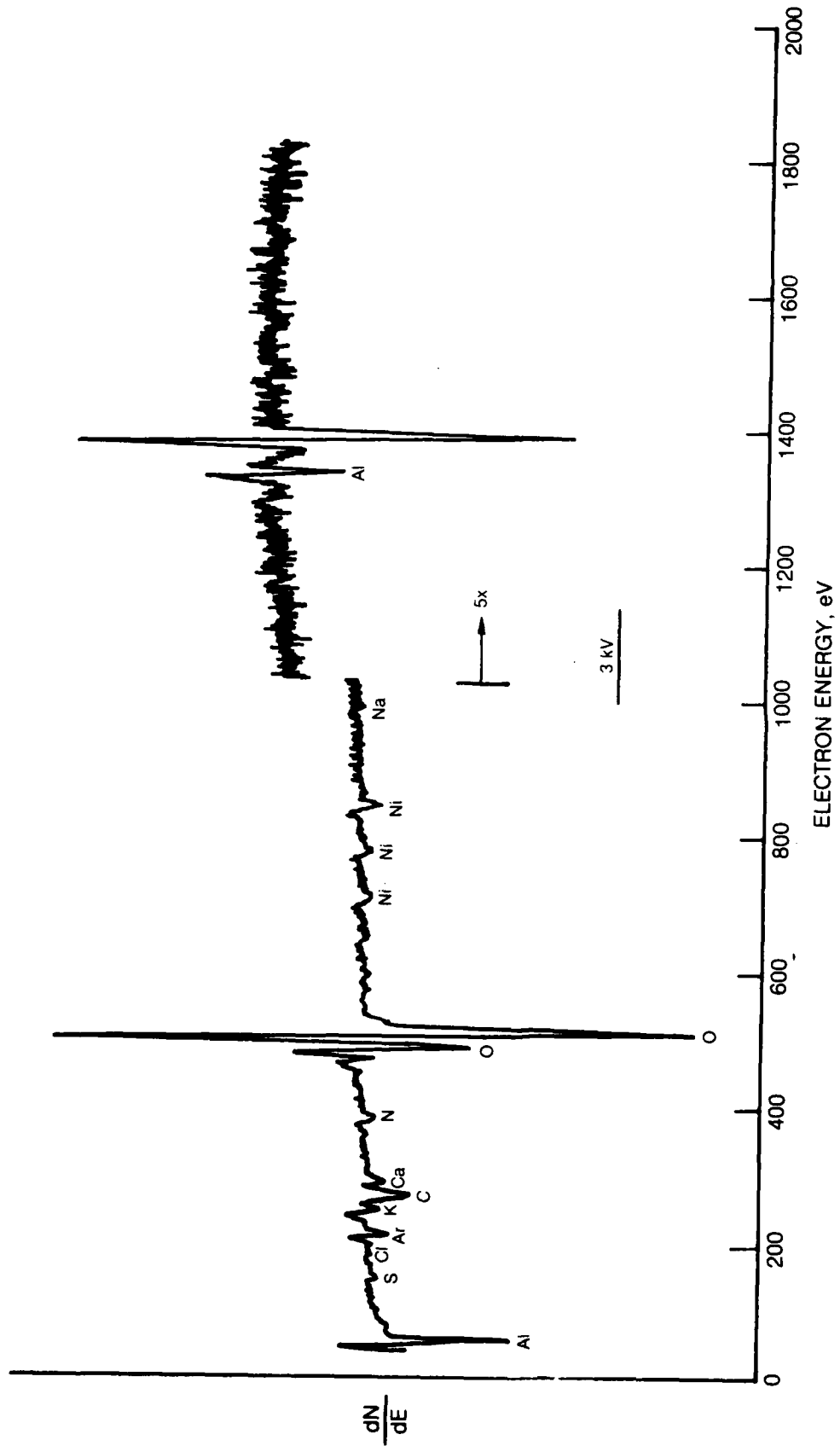
Figure 46. Auger Spectrum for Laser-Processed NiCrAl Heated to 700°C and Cooled
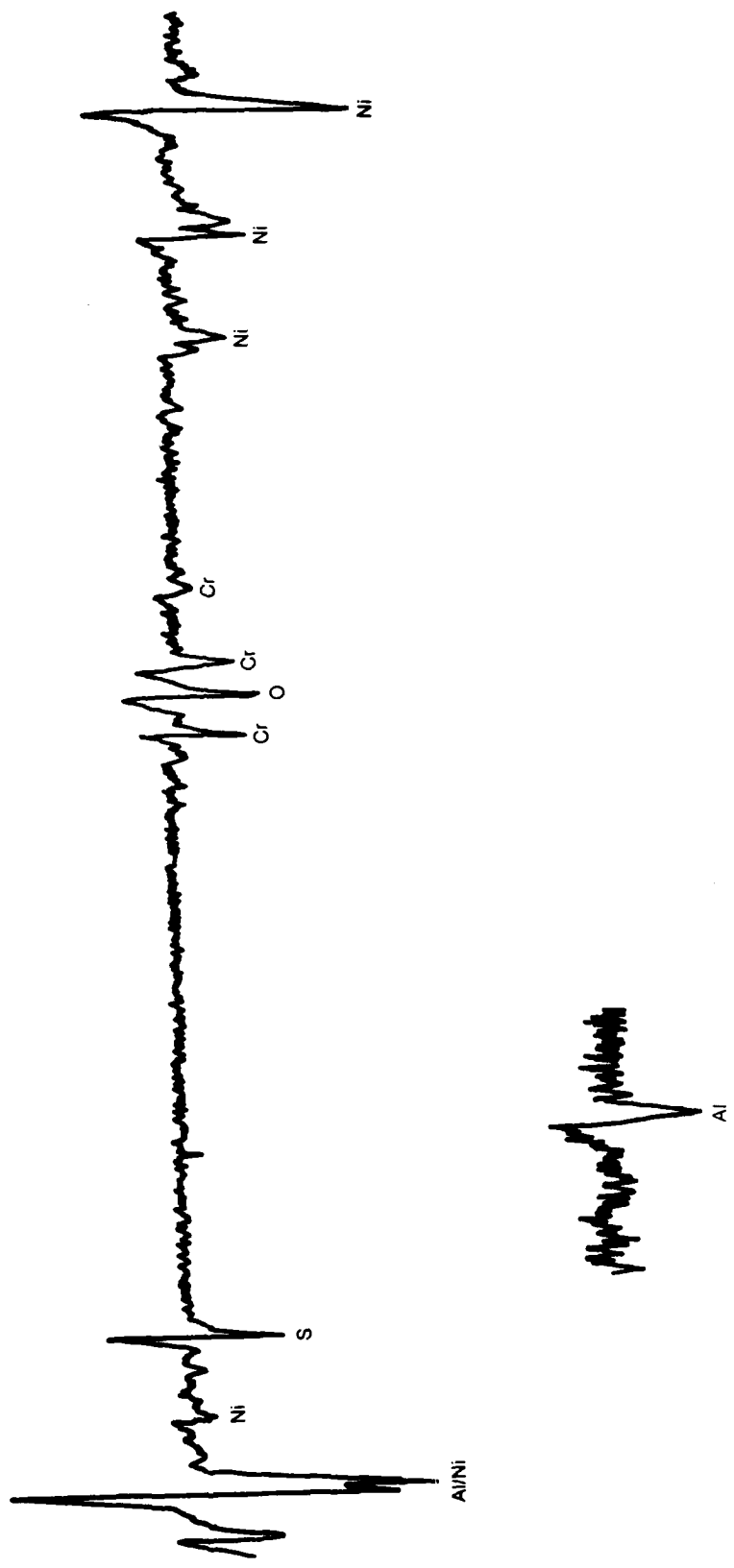
Figure 47. Auger Spectrum to NiCrAlY at 1000°C

83-10-11-6